Pamukkale Univ Muh Bilim Derg, 31(8), 1415-1430, 2025
(Special Issue of the 10th Geochemistry Symposium)

Pamukkale Üniversitesi Mühendislik Bilimleri Dergisi

Pamukkale University Journal of Engineering Sciences

Alteration geology and geochemistry of Kesikköprü (Bala, Ankara) Fe-skarn deposit

Kesikköprü (Bala, Ankara) Fe-skarn yatağının alterasyon jeolojisi ve jeokimyası

Mustafa Haydar Terzi[1], *Erkan Yılmazer*[1*]

[1]Department of Geological Engineering, Faculty of Engineering, Aksaray University, Aksaray, Türkiye.
mhaydarterzi@aksaray.edu.tr, erkanyilmazer@gmail.com

Received/Geliş Tarihi: 27.09.2025 Revision/Düzeltme Tarihi: 05.11.2025 doi: 10.65206/pajes.09599
Accepted/Kabul Tarihi: 06.11.2025 Special Issue Article/Özel Sayı Makalesi

Abstract

This study investigates the mineralogy of skarn, ore, and wall rocks in the Kesikköprü Fe-skarn deposit, along with the behavior, distribution, and enrichment processes of major oxides and trace elements. It also evaluates the skarn-forming potential of the Kesikköprü granitoid for different metals. The Kesikköprü mineralization is linked to an endoskarn zone dominated by garnet-pyroxene (±phlogopite±epidote) and to an exoskarn zone, in which assemblages toward the wall rocks comprise garnet (±pyroxene±phlogopite), pyroxene (±garnet±phlogopite±epidote), epidote-garnet, and epidote. Magnetite mineralization is particularly found within the epidote-garnet and epidote exoskarn subzones. Mineralogical and geochemical data indicate a significant increase in iron content during the late stages of skarn formation. Geochemical and isocon-mass balance analyses demonstrate a strong protolith control on skarn formation. In the granitoids, the endoskarn formation is characterized by Ca-Fe-Mg-Mn-Si addition with Al and alkalis (Na, K) depletion, whereas marbles record Ca depletion accompanied by increasing Fe input toward the ore zones. Based on the genetic link between skarn-forming granitoids and associated metal types, the Kesikköprü granitoid is inferred to have the potential to generate not only Fe-skarns but also Cu- and partially Au- and Pb-Zn skarns. Given the regional mineralization, these findings suggest that the Kesikköprü granitoid has multi-metal potential worthy of further exploration.

Keywords: Geochemistry, Raman, XRD, SEM-EDS, Skarn, Kesikköprü.

Öz

Bu çalışmada, Kesikköprü Fe-skarn yatağındaki skarn, cevher ve yan kayaçların mineralojisi ve bu kayaçlara ait ana oksit ve iz elementlerin davranışı, göreceli dağılımı ve zenginleşme süreçleri ile Kesikköprü granitoyidinin farklı metaller açısından skarn üretme potansiyeli incelenmiştir. Kesikköprü cevherleşmesi, granat-piroksen (±filogopit±epidot) ile baskın bir endoskarn zonu ve yan kayaçlara doğru granat (±piroksen±filogopit), piroksen (±granat±filogopit±epidot), epidot-granat ve epidot mineral birliktelikleri ile temsil olunan ekzoskarn zonları ile ilişkilidir. Manyetit cevherleşmesi özellikle epidot-granat ve epidot ekzoskarn alt zonlarında daha yoğundur. Mineralojik ve jeokimyasal özellikler, skarn oluşumunun geç evrelerinde demir içeriğinin belirgin bir şekilde arttığını göstermektedir. Jeokimyasal ve izokon-kütle dengesi analizleri, skarnların oluşumlarında ilksel yan kayaç (protolit) kontrolünün güçlü olduğunu ortaya koymaktadır. Granitoyidlerde, endoskarn gelişimi sırasında Ca-Fe-Mg-Mn-Si ilavesi ve Al ve alkali (Na, K) tükenmesi görülürken, mermerlerde cevher zonuna doğru Fe artışı ile birlikte Ca tüketilmesi görülmektedir. Skarn oluşturan granitoyidler ile metal türü arasındaki kökensel bağlantıdan hareketle Kesikköprü granitoyidinin, yalnızca Fe-skarnı değil, aynı zamanda Cu-, ve kısmen de Au- ve Pb-Zn skarnları oluşturma potansiyelinin var olduğu, bölgedeki cevherleşmeler düşünüldüğünde, Kesikköprü granitoyidinin çoklu metal üretme potansiyelinin olabileceği düşünülmektedir.

Anahtar kelimeler: Jeokimya, Raman, XRD, SEM-EDS, Skarn, Kesikköprü.

1 Introduction

The Kesikköprü Fe-skarn deposit geographically lies about 110 km southeast of Ankara (Türkiye); geologically, it occupies the northwestern sector of the Central Anatolian Crystalline Complex (CACC) [1] and falls within the Fe-skarn metallogenic belt defined by Kuşcu and Erler [2] (Figure 1a, b). The deposit formed at triple contacts among marble of the Central Anatolian Metamorphics (CAM) [1], gabbro and pyroxenite of the Central Anatolian Ophiolites (CAO) [1], and granite, granodiorite, and monzonite of the Central Anatolian Granitoids (CAG) [1],[3] (Figure 1b, c). Mining at Kesikköprü dates back to the 1960s; the deposit contains 12.7 million tonnes of reserves with ore grades of 39-61% Fe, 5-16 % SiO_2, and 0.58-1.8% S, and current production is on the order of 200-300 thousand tonnes of iron ore per year [4]. Most scientific and technical investigations in the area have been carried out by the General Directorate of Mineral Research and Exploration (MTA), focusing on the geology, economic status, feasibility, and resource development of the iron mineralization within the skarns [5]-[20]. Further studies have explored the mineralogy, petrography, and formation conditions of the skarns and iron mineralization, along with investigating the hydrothermal fluids responsible for their genesis [3],[21]-[26]. Among these, Yılmazer and Terzi [3] provided comprehensive evaluations of alteration patterns, host-rock geochemistry, and isotopic-geochronologic characteristics. However, none of the existing previous work has systematically examined the mineralogical and geochemical relationships among the skarn zones, the ore, and the wall rocks (the Kesikköprü granitoid, mafic-ultramafic rocks, and marble). Furthermore, no study has assessed the potential of the Kesikköprü granitoid to generate skarns with differing metal endowments. Given similar-age, geochemically

*Corresponding author/Yazışılan Yazar

comparable granitoid-related Fe-W, Fe, Pb-Zn, and Cu-Mo deposits nearby [27]-[29], and established links between granitoid geochemistry and skarn metal content [30]-[33], the Kesikköprü granitoid and skarn zones merit this kind of targeted study. Accordingly, this study; (i) characterizes the mineralogy of wall rocks, skarn and ore zones using Raman spectroscopy, X-ray diffraction (XRD), and scanning electron microscopy with energy-dispersive spectroscopy (SEM-EDS) methods, (ii) evaluates the behavior, relative distribution, and processes controlling the abundance of major oxides and trace elements in skarns, ore, and wall rocks, and (iii) assesses the capacity of the Kesikköprü granitoid to generate skarns with different metal endowments.

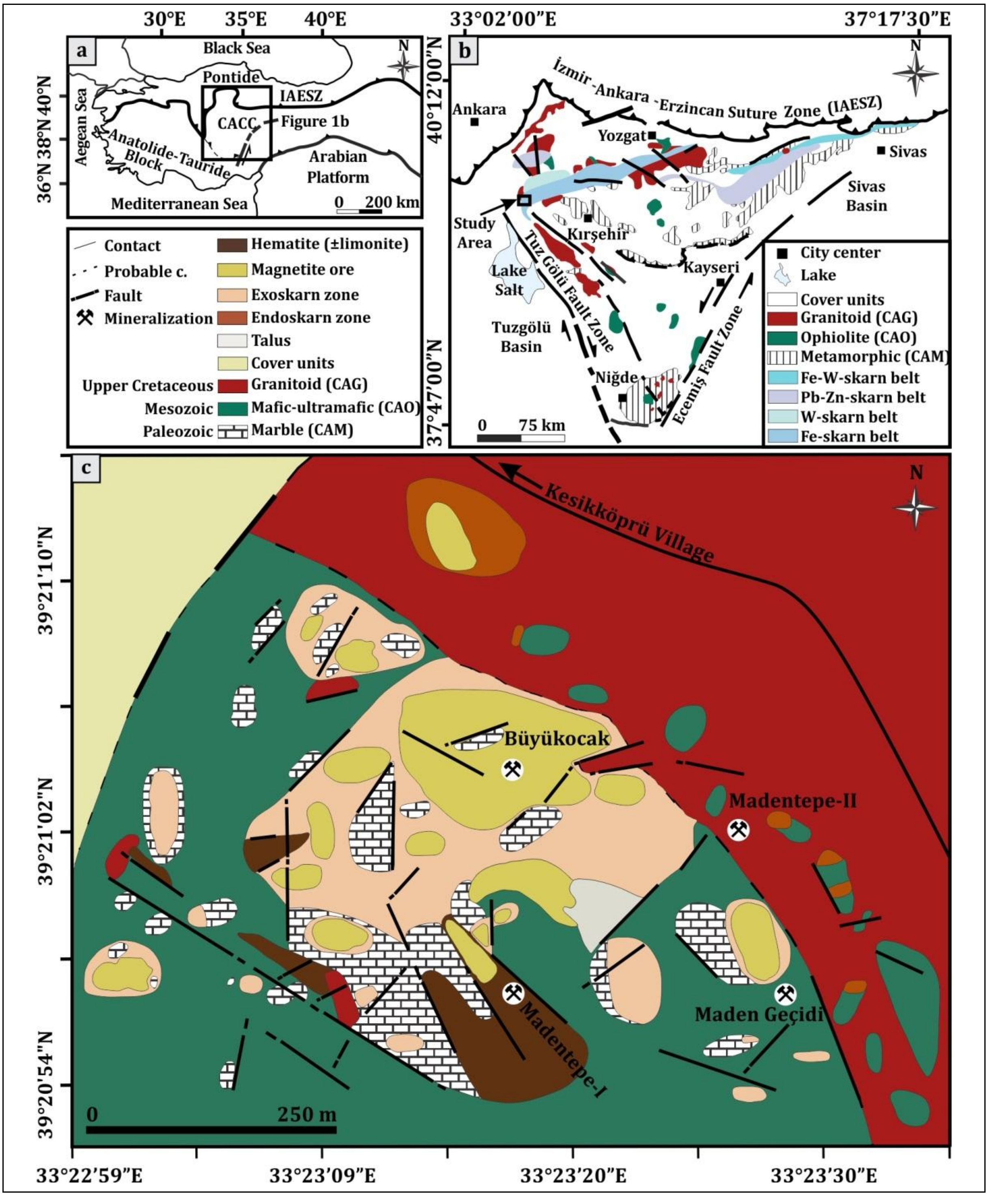

Figure 1. (a): Tectonic map of Türkiye showing the location of the CACC (simplified from [27]). (b): Simplified geological map of the CACC [2],[33]. (c): Geological and alteration map of the Kesikköprü Fe-skarn deposit (modified from [3]).

2 Materials and methods

This study was carried out in two stages: fieldwork and laboratory analyses. During fieldwork, an alteration map was created to document the relationships among wall rocks (Kesikköprü granitoid, mafic-ultramafic rocks, and marble), skarn zones, and mineralization (Figure 1c). Representative samples were collected for mineralogical-petrographic study, and thin-polished sections were prepared. Laboratory work consisted of four analytical methods: Raman spectroscopy, XRD, SEM-EDS, and wavelength-dispersive X-ray fluorescence spectrometry (WDXRF). Raman, XRD, and SEM-EDS analyses were performed at the Earth Sciences Application and Research Center (YEBİM) of Ankara University. Raman spectroscopy was conducted on six spots (one from mafic-ultramafic rock, two from endoskarn, and three from exoskarn zones) using a DXR 633 nm Filter Raman Microscope, and the obtained peaks were compared with reference spectra to identify mineral phases. XRD analyses were applied to seven samples (one mafic-ultramafic, two granitoids, one endoskarn, and three exoskarn zones), which were crushed, powdered, and analyzed with an Inel Equinox 1000 diffractometer equipped with a Co X-ray tube and a CPS-120 detector; diffractograms were converted to numerical values relative to a Cu cathode for comparison with ASTM standards, then processed with Match software for smoothing, baseline correction, and mineral identification. SEM-EDS analyses were performed on three thin sections from the exoskarn zone. WDXRF analyses were carried out at the Geochemical Analysis Laboratory (JAL) of the Scientific and Technological Application and Research Center (ASÜBTAM), Aksaray University, on 11 samples (4 granitoids, 6 exoskarns, and 1 ore sample) using a Malvern Panalytical Axios spectrometer; prior to measurement, powdered samples were mixed with a wax binder, pressed into pellets, and analyzed for major oxides and trace elements.

3 Geology

The CACC, also known as the Kırşehir Massif [34], is located in the northern part of the Anatolide-Tauride Platform and to the south of the İzmir-Ankara-Erzincan suture zone. It is generally composed of four main rock groups: (i) CAM, (ii) CAO, (iii) CAG, and (iv) cover units [1],[35],[36] (Figure 1a, 1b). The CAM constitutes the oldest units of the CACC and is tectonically overlain by ophiolitic rocks belonging to the CAO, which represent fragments of oceanic crust. These units are intruded by the CAG and, subsequently, by products of alkaline magmatism. The entire assemblage is unconformably overlain by sedimentary, volcanic, and pyroclastic rocks that constitute the cover units [1],[34]-[39] (Figure 1b).

In the Kesikköprü Fe-skarn deposit and its surroundings, the rock succession from oldest to youngest consists of metamorphics, mafic-ultramafic rocks, granitoids, and cover units. The metamorphic rocks, which represent the oldest lithology of the study area, include pure, clean marbles in the upper levels, underlain by alternations of marble, gneiss, and schist of varying thicknesses [21],[34]. However, gneiss and schist are not observed within the study area; instead, marbles occur as blocks enclosed in the mafic-ultramafic rocks [24],(Figure 1c). The marbles are mostly white to gray, with dolomitic varieties appearing darker. Their fractures, cracks, and foliation planes are commonly filled secondarily with carbonate, silica, magnetite, and sulfide minerals [3] (Figure 2a). Microscopically, the marbles are composed predominantly of medium- to coarse-grained, equigranular calcite, with minor dolomite and ankerite [3] (Figure 2b).

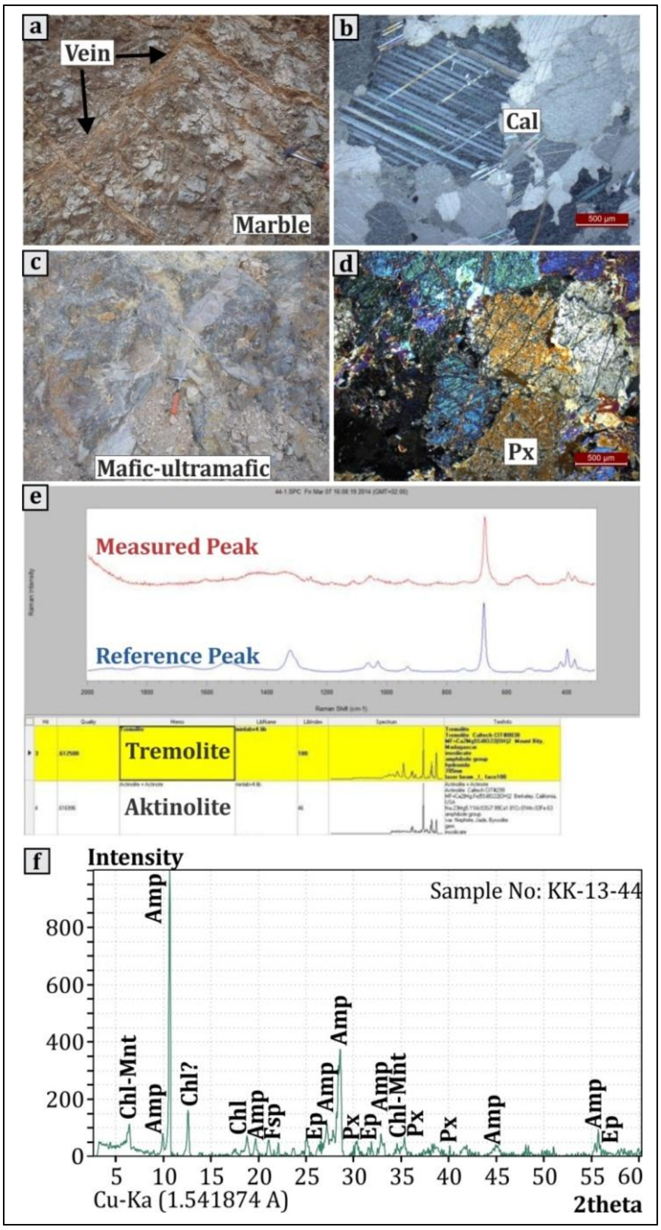

Figure 2. (a): Veins that contain calcite, quartz, and sulfide, cutting the marble. (b): Photomicrograph showing coarse-grained calcite mineral in marble (XPL). (c): Field photo from mafic-ultramafic rocks. (d): Photomicrograph of pyroxene in pyroxenite (XPL). (e): Raman spectra of tremolite. (f): XRD diffractogram of mafic-ultramafic rock (Amp: amphibole; Ep: Epidote; Fsp: feldspar; Cal: Calcite; Chl-Mnt: Chlorite-montmorillonite; Px: Pyroxene).

The mafic-ultramafic rocks, which tectonically overlie the metamorphic assemblages within the CACC, are widely exposed throughout the study area. Mafic-ultramafic rocks in the Kesikköprü region are interpreted as regional equivalents of the Ankara Mélange and the Karakaya ultramafics [21],[25],[26],[34],[40]. This unit is composed of pyroxenite, hornblendite, and gabbros [21],[24]. Owing to intense deformation, the contact relationships among these lithologies could not be clearly delineated. The mafic-ultramafic rocks, which are characteristically dark-colored, chiefly consist of plagioclase, clinopyroxene, orthopyroxene, and amphibole [3] (Figure 2c, f). Alteration types such as carbonatization, silicification, uralitization, chloritization, and epidotization are commonly observed in these rocks (Figure 2f).

Granitoid intrusion that crosscuts the metamorphic and mafic-ultramafic rocks was initially described by Bayhan [41] as the “Çelebi Granitoid” (Figure 3a).

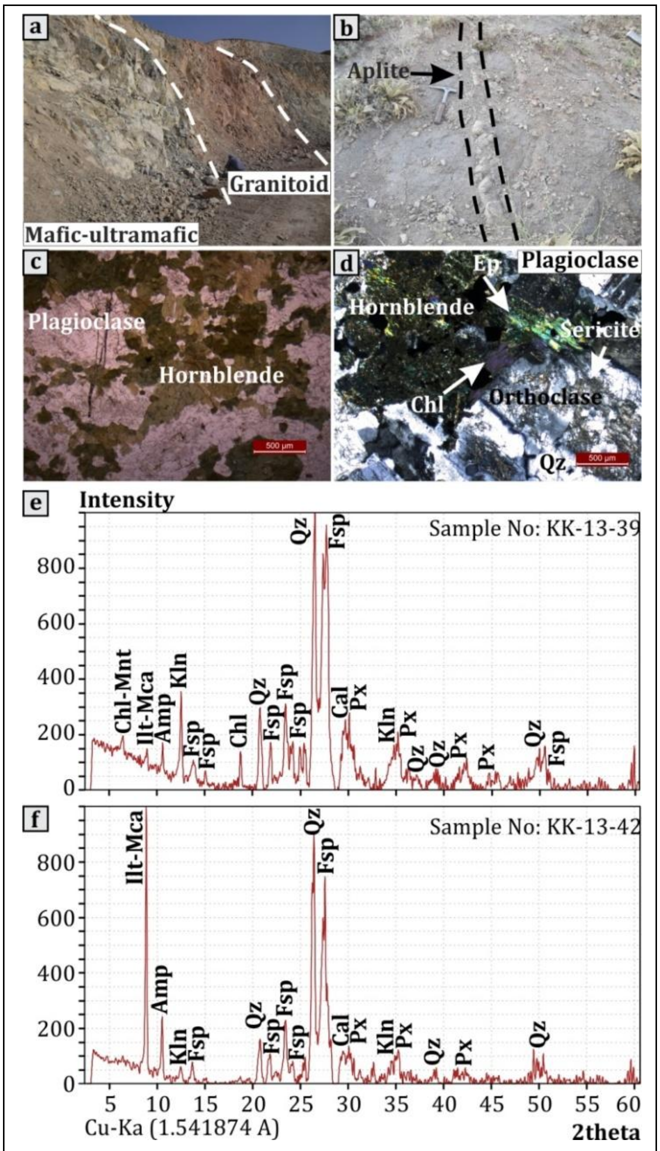

Figure 3. (a): Field photo from granitoid cutting the mafic-ultramafic rocks. (b): Aplite dyke cutting granitoid. (c): Microphotograph of hornblende and plagioclase minerals in granodiorite (PPL). (d): Microphotograph showing sericitization, chloritization, and epidotization in monzonite (XPL). (e-f): XRD diffractograms of granitoid (Amp: amphibole; Cal: calcite, Chl-Mnt: chlorite-montmorillonite; Fsp: feldspar; Ilt-Mca: illite-mica, Kln: kaolinite, Px: pyroxene; Qz: quartz).

However, due to their widespread occurrence in the Kesikköprü area southwest of Çelebi, they were later named as the “Kesikköprü Granitoid” by Doğan [25] and Doğan et al. [3],[26]. These granitoids, typically gray to pinkish-gray in color and phaneritic in texture, contain enclaves of monzonite, monzodiorite, quartz-diorite, and diorite compositions, as well as xenoliths of mafic-ultramafic rocks, and are locally crosscut by aplite dykes [3],[21] (Figure 3b). In thin sections, the granitoid samples display holocrystalline-granular to holocrystalline-porphyritic textures and comprise granite, granodiorite, and monzonite compositions [21]. Their mineral assemblage includes plagioclase, orthoclase, quartz, hornblende, biotite, clinopyroxene, titanite, and apatite [3] (Figure 3c, f). Alteration features, particularly pronounced near the skarn zones, include kaolinization, sericitization, uralitization, chloritization, and epidotization (Figure 3e, f).

4 Mining geology

Alteration at the Kesikköprü deposit comprises endoskarn and exoskarn zones (Figure 1c). The endoskarn, hosted within the granitoids, is characterized by garnet-pyroxene (±phlogopite±epidote) assemblages, whereas the exoskarn, which develops toward the wall rocks, is subdivided into four mineralogically distinct subzones: garnet (±pyroxene±phlogopite), pyroxene (±garnet±phlogopite ±epidote), epidote-garnet, and epidote [3].

Endoskarn zones occur as accumulations and veins within granitoids. Most garnets in this zone are isotropic, medium- to coarse-grained, and anhedral, while pyroxenes, showing weak pleochroism, occur as anhedral to subhedral grains (Figure 4a, b). In the endoskarn zone, phlogopite is relatively fine-grained compared with that in the exoskarn zones and occurs in variable amounts with magnetite and pyrite as veins and patches (Figure 4b). Epidote predominantly occurs as a replacement product of garnet [3],[24]. Phlogopite is observed to have undergone widespread chloritization under microscopic examination, and the presence of montmorillonite and vermiculite is confirmed by XRD analyses. This zone may also contain variable amounts of magnetite, pyrite, quartz, and calcite (Figure 4c-e).

The exoskarn zone is more extensive and displays mineralogical zonation outward from the intrusive contact, compared to the endoskarn zone [3] (Figure 1c). The garnet (±pyroxene±phlogopite) exoskarn subzone consists largely of medium- to coarse-grained, subhedral-euhedral garnet that is dominantly isotropic with locally anomalous anisotropy, with lesser pyroxene and phlogopite (Figure 5a-c). Pyroxenes are most commonly preserved phases between garnets. Compared with the endoskarn zone, phlogopite is coarser-grained. Epidotization, tremolitization, and chloritization commonly affect garnet, pyroxene, and phlogopite (Figure 5b, d). Whole-rock XRD analysis shows a chlorite-montmorillonite-vermiculite signal indicating retrograde hydrothermal alteration of Fe-Mg silicates (Figure 4e and Figure 5e). This subzone lacks wall rock relicts and exhibits more intense alteration.

The pyroxene (±garnet±phlogopite±epidote) exoskarn subzone is characterized by an increase in fine-grained, subhedral-euhedral pyroxenes and the presence of anisotropic, zoned euhedral garnet [3] (Figure 6a). Along with pyroxene and grandite-series (grossular-andradite) garnet, this subzone also contains phlogopite, epidote, calcite, and magnetite (Figure 6a-c). The powder XRD pattern is dominated by calcite, with subordinate clinopyroxene and weak garnet and magnetite reflections (Figure 6d). Toward the wall rocks, retrograde alteration intensifies, leading to a marked decrease in pyroxene abundance, while garnet abundance continues to diminish gradually.

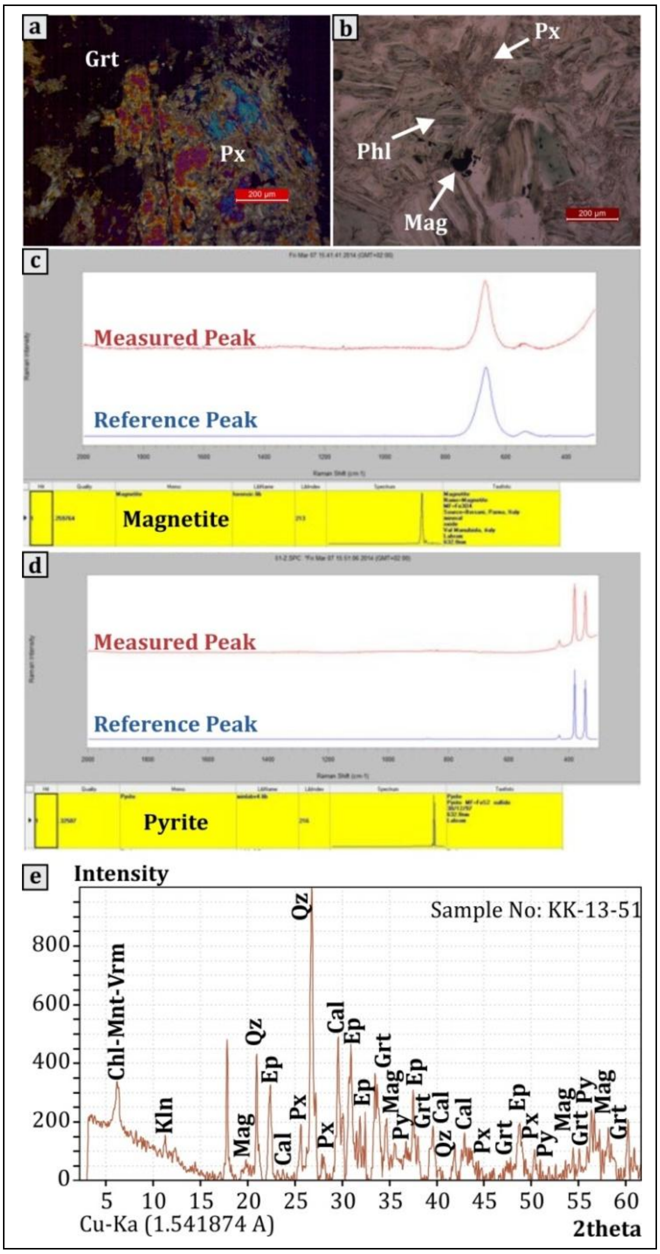

Figure 4. (a-b): Photomicrograph showing the mineral association of garnet, pyroxene, phlogopite, and magnetite in the endoskarn zone. (a): XPL. (b): PPL. (c-d): Raman spectra of magnetite and pyrite. (e): XRD diffractogram of the endoskarn zone (Cal: calcite, Chl-Mnt-Vrm: chlorite-montmorillonite-vermiculite; Ep: epidote; Grt: garnet; Kln: kaolinite; Mag: magnetite; Phl: phlogopite; Px: pyroxene; Py: pyrite; Qz: quartz).

The epidote-garnet exoskarn subzone is characterized by coarser-grained epidote than in the other exoskarn subzones, whereas garnet is medium- to fine-grained and less abundant than in the pyroxene (±garnet±phlogopite±epidote) exoskarn subzone (Figure 7a). This subzone occurs farther from the granitoid and closer to the wall rocks. Relics of unmetasomatized marble are commonly observed in this zone [3] (Figure 7b). Garnet exhibits optical anisotropy consistent with Fe and Al zoning/variation (Figure 7c). Magnetite, pyrite, quartz, calcite, and phlogopite may be present. The XRD pattern shows abundant garnet with epidote, calcite, quartz, and magnetite, consistent with local garnet-rich bands within this subzone (Figure 7d). The epidote exoskarn subzone is defined by the absence or near-absence of garnet and is dominated by fine- to medium-grained epidote [24] (Figure 7e). Calcite, quartz, pyrite, and magnetite are also present in this subzone.

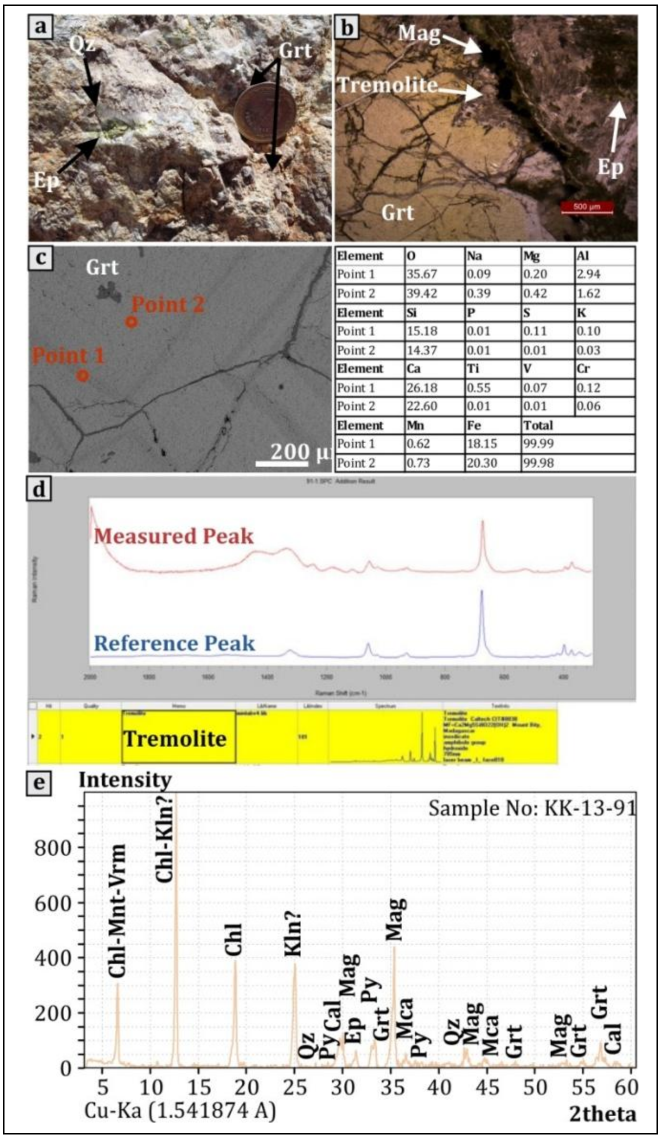

Element	O	Na	Mg	Al
Point 1	35.67	0.09	0.20	2.94
Point 2	39.42	0.39	0.42	1.62
Element	Si	P	S	K
Point 1	15.18	0.01	0.11	0.10
Point 2	14.37	0.01	0.01	0.03
Element	Ca	Ti	V	Cr
Point 1	26.18	0.55	0.07	0.12
Point 2	22.60	0.01	0.01	0.06
Element	Mn	Fe	Total	
Point 1	0.62	18.15	99.99	
Point 2	0.73	20.30	99.98	

Figure 5. (a): Coarse-grained and subhedral-euhedral garnets in the exoskarn subzone. (b): Microphotograph showing the mineral association of garnet, epidote, tremolite, and magnetite (PPL). (c): BSE image of zoned garnet and SEM-EDS results. (d): Raman spectra identifying tremolite. (e): Powder XRD pattern of the garnet (±pyroxene±phlogopite) exoskarn subzone (Cal: calcite; Chl-Mnt-Vrm: chlorite-montmorillonite-vermiculite; Ep: epidote; Grt: garnet; Kln: kaolinite; Mag: magnetite; Mca: mica; Qz: quartz, Py: pyrite).

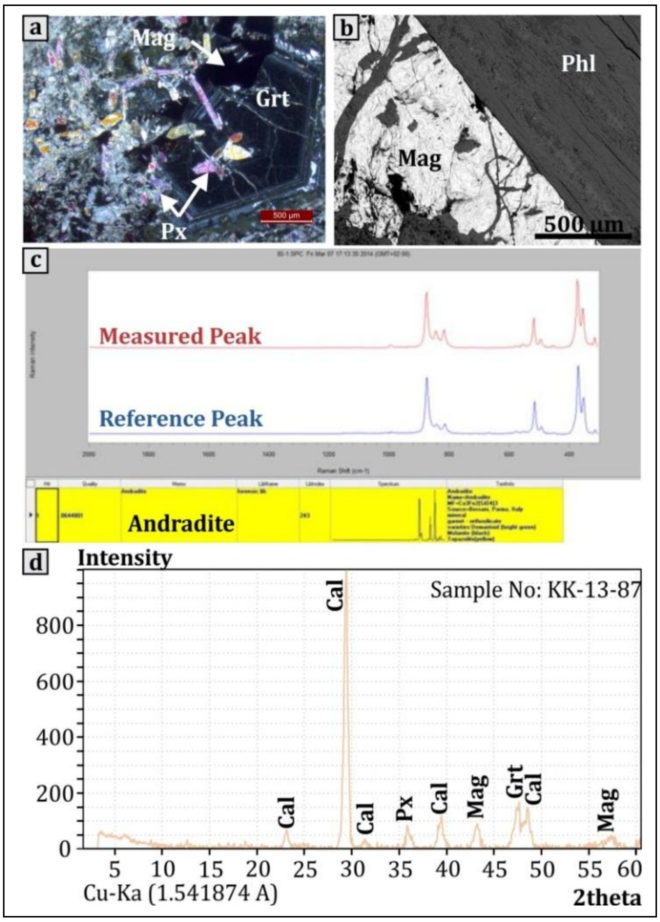

Figure 6. (a): Photomicrograph (XPL) of the pyroxene (±garnet±phlogopite±epidote) exoskarn subzone showing subhedral-euhedral pyroxene and euhedral zoned garnet. (b): BSE image of magnetite adjacent to phlogopite. (c): Raman spectrum identifying andradite. (d): Powder XRD pattern of the same exoskarn subzone (Cal: calcite; Grt: garnet; Mag: magnetite; Phl: phlogopite; Px: pyroxene).

In the Kesikköprü region, Fe-skarn mineralization is classified into two categories: oxide ores, including magnetite and hematite with minor limonite, and sulfide ores dominated by pyrite, chalcopyrite, and marcasite [3],[24]. Magnetite mineralization occurs as vein- and disseminated-type in endoskarn, and as banded, massive, and brecciated textures in exoskarns [3]. Magnetite can be found throughout all skarn zones in variable amounts. Economic massive magnetite mineralization is especially concentrated in the epidote-garnet and epidote exoskarn subzones, where coarse-grained phlogopite commonly accompanies magnetite (Figure 8a, b). Microscopically, magnetite appears grayish and in some locations has been partially replaced by hematite through martitization [3]. Sulfide mineralization, occurring as veins, accumulations, and disseminations, crosscuts the magnetite ores (Figure 8c). Microscopically, pyrite appears cream to pale yellow, and generally subhedral-euhedral (Figure 8d). In some cases, pyrite rims have altered to marcasite [3]. Both magnetite and sulfide mineralization are partially oxidized near the upper levels of the deposit, where they are replaced by hematite (±limonite) and malachite, depending on the intensity of oxidation processes. The distribution of these zones in the open pit is structurally controlled by fracture-fault systems [3],[24].

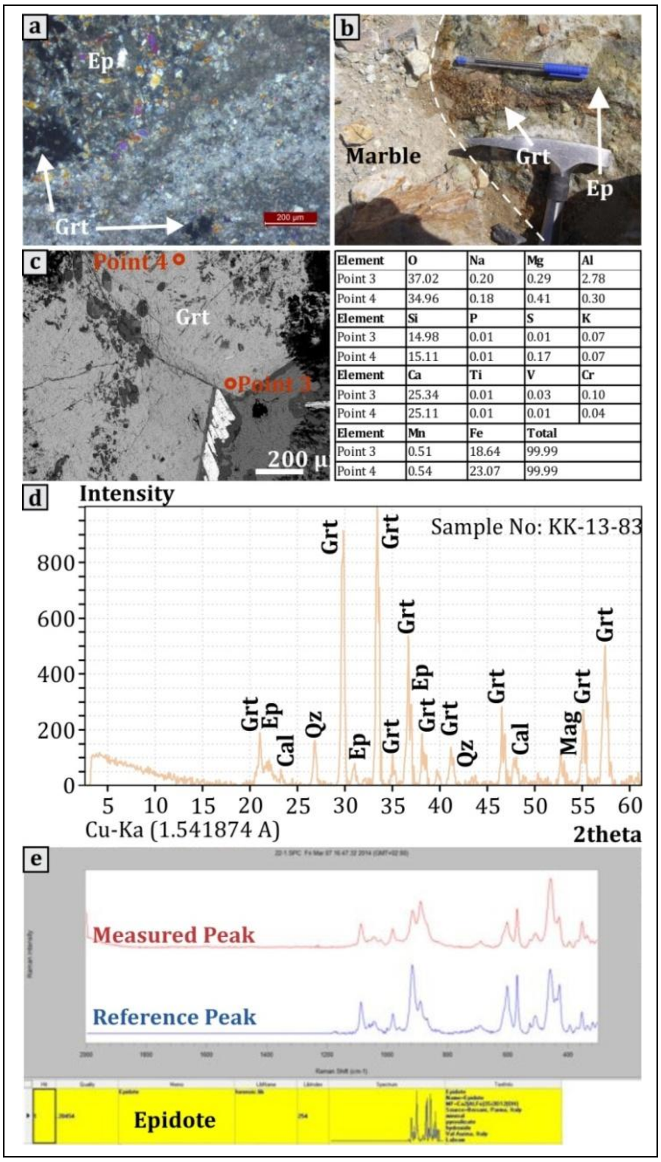

Element	O	Na	Mg	Al
Point 3	37.02	0.20	0.29	2.78
Point 4	34.96	0.18	0.41	0.30
Element	Si	P	S	K
Point 3	14.98	0.01	0.01	0.07
Point 4	15.11	0.01	0.17	0.07
Element	Ca	Ti	V	Cr
Point 3	25.34	0.01	0.03	0.10
Point 4	25.11	0.01	0.01	0.04
Element	Mn	Fe	Total	
Point 3	0.51	18.64	99.99	
Point 4	0.54	23.07	99.99	

Figure 7. (a): Microphotograph of the epidote-garnet exoskarn subzone (XPL). (b): Epidote and garnet vein in marble. (c): BSE image of garnet and SEM-EDS result. (d): XRD diffractogram of the epidote-garnet exoskarn subzone. (e) Raman spectrum of epidote in the epidote exoskarn subzone (Cal: calcite; Ep: epidote; Grt: garnet; Mag: magnetite; Qz: quartz).

5 Results

5.1 Alteration geochemistry

5.1.1 Isocon diagrams

Alteration geochemistry studies were conducted at the Kesikköprü Fe-skarn deposit to evaluate the geochemical impacts of hydrothermal alteration and to quantify net mass gains and losses between altered and fresh wall rocks. To assess metasomatic changes, isocon diagrams and corresponding mass-balance calculations were prepared for six protolith-alteration pairs: granitoid vs endoskarn, granitoid vs ore, marble vs exoskarn, marble vs ore, mafic-ultramafic vs exoskarn, and mafic-ultramafic vs ore [42].

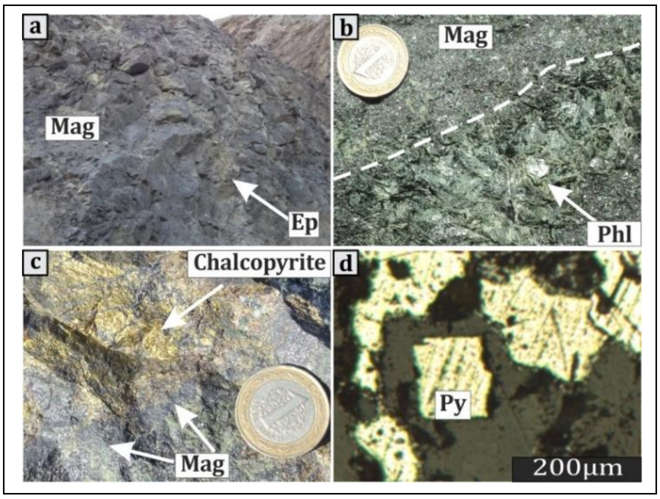

Figure 8. (a): Field photo from massive magnetite mineralization. (b): Coarse-grained phlogopites accompanying magnetite. (c): Chalcopyrite cutting magnetite. (d): Microphotograph of euhedral pyrites (Ep: epidote; Mag: magnetite; Phl: phlogopite; Py: pyrite).

The dataset comprises 31 granitoid samples, 10 mafic-ultramafic samples, 1 marble sample, 6 endoskarn samples, 22 exoskarn samples, and 2 ore samples. Of these, 4 granitoid samples, 6 exoskarn samples, and 1 ore sample were newly analyzed in this study. The remaining analyses were compiled to include all analyses reported by Terzi [24] and Yılmazer & Terzi [3], excluding the marble samples KK-13-61 and KK-13-74 reported by Terzi [24] (Table 1). Statistical results for all data are given in Table 2. To stabilize isocon slopes and reduce scatter introduced by heterogeneity in alteration intensity and veinlet contributions, we used the mean lithology compositions of all data rather than single-sample values (Table 2). Using lithology-based averages provides a more representative chemical signature of the protolith, increases the reliability of the isocon slope, and minimizes deviations in the calculated gain/loss of samples.

The granitoid-endoskarn pair shows $C^{o} = 0.73$, consistent with bulk mass addition to the intrusion during endoskarn alteration (Table 3 and Figure 9a). This addition is carried primarily by Ca, Fe, Mg, Mn, and Si: CaO (+18.15), Fe_2O_3 (+8.64), MgO (+9.09), MnO (+0.18), and SiO_2 (+6.33), with concomitant leaching of alkalis (Na_2O −2.26; K_2O −4.26) and moderate Al loss (Al_2O_3 −1.62). The trace-elements such as Rb (−153.83), Ba (−911.28), and Cu (−19.69) show depletions in the endoskarn zones, whereas Zn (+35.07), Ni (+181.25), Co (+20.27), and V (+35.07) are enriched. Sr (+232.6) increases coherently with Ca addition. Ti shows negligible change (+0.10 as TiO_2), validating Zr suitability as immobile reference points for the isocon.

In the granitoid-ore pair, $C^{o} = 0.06$ is represented by extreme mass addition during ore formation (Table 3 and Figure 9b), with large increases in some of the major oxide and trace elements, notably Fe_2O_3 (+1155.57), MnO (+68.69), CaO (+165.35), and strong enrichments in chalcophile and transition metals (e.g., Pb +4742.41; Zn +1949.15; Cu +722.42; Co +1780.85; Ni +228.14; V +253.45).

The exoskarn-marble pair is marked by a steep isocon ($C^{o} = 5.99$), indicating bulk mass loss (Table 3 and Figure 9c). The mass-balance calculation records an important CaO loss (−51.45), accompanied by small gains in Fe_2O_3 (+2.77). Large Ion Lithophile Elements (LILE) are depleted (Ba:−14.94; Sr:−60.11; Pb:−14.33), whereas Cu is slightly added (+8.03). V (−30.63) and Ni (−52.89) are notably removed. Ti remains essentially immobile (TiO_2 −0.01), confirming the robustness of the isocon construction.

Progression into the ore zone is marked by Fe addition: Fe_2O_3 increases by +28.45, while CaO continues to decrease (−50.84) and MgO slightly rises (+0.57). The isocon slope ($C^{o} = 2.3$) indicates "net mass loss". Compared with the exoskarn-marble pair, base-metal enrichment becomes more pronounced, with Zn (+38.73), Pb (+82.38), and Co (+16.81) recording positive gains, while Ba (−18), V (−27.84), Ni (−52.92), and Sr (−19.75), are notably depleted (Table 3 and Figure 9d).

Alteration of mafic-ultramafic rocks shows a different buffering regime and metal inventory. In the mafic-ultramafic vs exoskarn diagram, $C^{o} = 0.71$ indicates bulk mass gain, dominated by Fe and Ca addition (Fe_2O_3 +34.7; CaO +19.28), with losses of SiO_2 (−9.08), Al_2O_3 (−7), and MgO (−4.57) (Table 3 and Figure 9e). Trace element signatures include strong additions of Co (+85.25), Cu (+131.6), Pb (+236.06), As (+243.41), and modest Nd (+53.77), Th (+15.94), and Zn (+19.16), whereas Ni (−52.93), Ba (−42.38), Sr (−30.58), and V (−134.85), show a net loss.

The ore vs mafic-ultramafic rocks pair is the extreme in terms of metal budget. With $C^{o} = 0.27$, the system experienced substantial bulk mass addition (Table 3 and Figure 9f). Fe_2O_3 shows a dramatic gain (+251.78), accompanied by increases in CaO (+24.42) and MnO (+15.20), and large losses of SiO_2 (−32.05), Al_2O_3 (−10.51), and moderate MgO (−5.06). Some of the trace elements are exceptionally enriched: Zn (+386.45), Cu (+145.25), Pb (+1053.56), and Co (+352.16) all show large positive balances, while Ni (−53.16), V (−111.26), and Ba (−68.25) are depleted. Sr is also strongly added (+310.53).

5.1.2 Geochemical variations across skarn zones at Kesikköprü

To assess elemental mobility among granitoid, endoskarn, ore, exoskarn zones, and wall rocks, we also examined variations in mean major oxide and trace element compositions along a representative cross section of the deposit (Table 2 and Figure 10). Consistent with the isocon diagrams, SiO_2, Al_2O_3, Na_2O, and K_2O show a decrease from granitoid toward the endoskarn and ore zones, whereas Fe_2O_3, MnO, and to a lesser extent CaO increase. Sr and Ni reach their highest mean concentrations in the endoskarn zone. The ore zone, compared with skarn zones and wall rocks, is also enriched in Pb, Zn, Co, Sn, and Mo alongside Fe_2O_3 and MnO. From the ore zone toward the exoskarn zone, SiO_2, Al_2O_3, MgO, CaO, Cu, Ni, U, and As increase, while Fe_2O_3, MnO, Pb, Zn, Co, Sn, and Mo decrease. The exoskarn zone yields the highest Cu and As mean contents. From the exoskarn zone toward marble, CaO content increases, in contrast with many trace elements except for Y and Ni (Figure 10). Collectively, these trends are governed by wall rock lithology, the mineralogy of the skarn zones, and the extent to which specific major oxides and trace elements participate in calc-silicate metasomatic reactions.

Table 1. Geochemistry of wall rocks and skarn samples from the Kesikköprü Fe-skarn deposit.

Sample No	Rock/Alteration	SiO_2 %	TiO_2 %	Al_2O_3 %	Fe_2O_3 %	MnO %	MgO %	CaO %	Na_2O %	K_2O %	P_2O_5 %	Ba ppm	Rb ppm	Sr ppm	Y ppm	Zr ppm	Nb ppm
KK-20-01	Granitoid	58.3	0.63	14.9	6.4	0.1	3.7	6.5	1.95	4.49	0.23	991	156	497	39	137	5
KK-20-06	Granitoid	59.9	0.39	14.2	5.6	0.2	2.5	5.9	1.95	4.62	0.21	796	181	477	45	157	7
KK-20-08	Granitoid	64.0	0.26	15.4	4.5	0.1	2.3	4.7	2.42	4.63	0.16	816	168	456	43	167	7
KK-20-09	Granitoid	65.3	0.25	15.6	4.3	0.1	1.8	4.5	2.42	4.78	0.15	878	171	427	40	157	7
KK-18-01	Exoskarn	18.1	-	0.6	53.3	0.3	1.2	20.1	0.05	0.02	0.00	-	4	20	-	14	2
KK-18-07	Exoskarn	36.5	0.91	14.2	13.7	0.3	5.4	22.0	0.09	0.01	0.15	39	5	1081	4	132	-
KK-18-10	Exoskarn	27.2	0.09	4.5	22.4	0.5	6.2	31.4	0.15	-	0.03	-	-	66	-	22	2
KK-18-11	Exoskarn	35.4	0.01	1.2	30.0	0.7	1.1	28.5	0.07	-	0.01	-	-	21	3	15	3
KK-18-14	Exoskarn	25.2	0.01	10.6	35.8	0.5	16.2	3.3	0.04	0.05	0.00	-	3	13	-	15	2
KK-18-18	Exoskarn	26.9	0.05	10.8	31.7	0.4	16.5	4.9	0.12	0.04	-	-	5	38	-	17	3
KK-20-04	Ore (Magnetite)	0.7	0.03	0.2	62.1	8.1	0.4	17.9	0.09	0.06	0.01	-	6	249	-	20	1

Sample No	Rock/Alteration	Th ppm	Pb ppm	Zn ppm	Cu ppm	Ni ppm	Co ppm	U ppm	Sn ppm	Mo ppm	As ppm	Nd ppm	Sm ppm	V ppm	Na_2O+K_2O ppm	Rb/Sr
KK-20-01	Granitoid	9	53	68	24	31	31	12	2	5	17	42	7	1	6.45	0.31
KK-20-06	Granitoid	15	51	67	15	10	26	13	3	4	15	39	9	-	6.57	0.38
KK-20-08	Granitoid	20	43	50	14	9	23	13	3	5	14	30	9	-	7.05	0.37
KK-20-09	Granitoid	20	41	43	42	9	30	13	4	5	12	31	8	-	7.20	0.40
KK-18-01	Exoskarn	10.3	582.1	39.1	1440.1	19.4	248.5	8.4	1.7	-	103.4	58.0	-	-	0.07	0.17
KK-18-07	Exoskarn	24.2	69.5	38.9	3.5	11.0	40.1	8.7	-	1.5	12.4	64.0	1.0	-	0.10	0.01
KK-18-10	Exoskarn	114.1	212.4	84.0	15.4	10.3	67.1	8.5	-	-	39.6	79.7	-	-	0.15	-
KK-18-11	Exoskarn	16.9	562.5	55.3	84.5	44.5	109.3	8.5	-	-	110.1	83.6	-	-	0.07	-
KK-18-14	Exoskarn	-	2.1	118.2	5.4	1.9	215.8	8.4	-	-	-	-	-	-	0.10	0.26
KK-18-18	Exoskarn	0.4	7.8	148.6	8.7	289.5	206.2	8.4	-	-	-	8.1	-	-	0.17	0.13
KK-20-04	Ore (Magnetite)	4.0	291.0	192.0	45.3	14.7	166.0	8.4	22.2	-	33.0	82.3	-	-	0.16	0.02

Table 2. Descriptive statistical values of wall rocks and skarn samples from Kesikköprü Fe-skarn deposit [3],[24],[This study].

Rock/Alteration		SiO_2 %	TiO_2 %	Al_2O_3 %	Fe_2O_3 %	MnO %	MgO %	CaO %	Na_2O %	K_2O %	P_2O_5 %	Ba ppm	Rb ppm	Sr ppm	Y ppm	Zr ppm	Nb ppm
Marble	KK-13-35	5.8	0.03	0.6	2.2	0.3	0.3	55.3	0.08	0.01	0.004	19.3	1.1	76.9	12.5	4.7	3.8
	Sample	1	1	1	1	1	1	1	1	1	1	1	1	1	1	1	1
Mafic-Ultramafic	Minimum	46.8	0.1	1.5	0.7	0.02	6.2	9.9	0.1	0.2	0.01	25.0	1.0	12.0	3.0	8.4	0.9
	Maximum	57.1	0.7	19.5	10.3	0.19	18.1	19.9	2.4	1.5	0.13	246.3	76.2	355.8	16.2	163.8	7.5
	Mean	51.7	0.3	12.2	7.0	0.14	12.1	13.5	0.7	0.6	0.04	79.3	17.6	172.5	8.4	39.7	4.0
	Sample	10	10	10	10	10	10	10	10	10	10	10	10	10	10	10	10
Granitoid	Minimum	58.2	0.2	13.8	1.8	0.01	0.7	2.6	1.8	1.5	0.1	291.8	40.8	248.0	12.0	136.3	4.9
	Maximum	69.1	0.7	17.3	6.6	0.2	4.7	6.6	3.4	5.7	0.3	1249.0	213.2	534.9	44.9	267.0	21.2
	Mean	63.2	0.5	15.4	4.4	0.1	2.2	4.5	2.7	4.6	0.2	981.0	161.1	427.4	21.6	178.1	13.5
	Sample	31	31	31	31	31	31	31	31	31	31	31	31	31	31	31	31
Endoskarn	Minimum	47.7	0.2	3.1	6.9	0.1	2.1	13.5	0.1	0.1	0.04	10.0	1.5	67.0	4.8	32.1	3.6
	Maximum	56.2	0.7	11.9	12.8	0.2	17.4	21.0	1.2	0.5	0.21	108.0	11.2	906.1	16.9	228.8	15.1
	Mean	51.0	0.4	10.1	9.6	0.2	8.3	16.6	0.3	0.3	0.12	51.2	5.3	484.2	12.9	130.7	10.1
	Sample	6	6	6	6	6	6	6	6	5	6	6	6	6	6	6	6
Exoskarn	Minimum	2.0	0.003	0.02	0.8	0.1	0.4	3.3	0.04	0.01	0.003	3.0	0.6	4.3	0.9	0.9	0.6
	Maximum	55.6	0.9	17.0	61.1	0.7	16.5	57.6	0.2	2.1	0.1	193.3	97.6	1081.2	24.9	153.4	33.8
	Mean	30.2	0.1	3.7	29.5	0.4	5.4	23.2	0.1	0.2	0.03	26.1	8.1	100.6	4.8	28.2	6.0
	Sample	22	21	22	22	22	22	22	22	18	21	16	20	22	18	22	21
Ore (Magnetite)	Minimum	0.7	0.02	0.2	62.1	0.3	0.4	2.7	0.05	0.01	0.01	3.0	0.4	14.0	0.8	1.8	0.6
	Maximum	10.1	0.03	0.7	78.9	8.1	3.4	17.9	0.09	0.06	0.01	3.0	5.8	249.4	0.8	19.9	0.6
	Mean	5.4	0.02	0.5	70.5	4.2	1.9	10.3	0.07	0.04	0.01	3.0	3.1	131.7	0.8	10.8	0.6
	Sample	2	2	2	2	2	2	2	2	2	2	1	2	2	1	2	2

Rock/Alteration		Th ppm	Pb ppm	Zn ppm	Cu ppm	Ni ppm	Co ppm	U ppm	Sn ppm	Mo ppm	As ppm	Nd ppm	Sm ppm	V ppm	Na_2O+K_2O ppm	Rb/Sr
Marble	KK-13-35	3	43.9	13.8	10.0	59.3	30.8	11.0	1.1	3.5	1.6	-	-	37.0	0.084	0.01
	Sample	1	1	1	1	1	1	1	1	1	1	-	-	1	1	1
Mafic-Ultramafic	Minimum	0.2	2.0	21.6	1.0	1.0	25.9	0.2	0.9	2.8	3.3	6.1	1.8	73.3	0.46	0.02
	Maximum	12.0	57.6	147.2	64.4	275.7	77.1	17.6	3.4	12.1	35.3	6.1	1.8	334.0	2.91	0.52
	Mean	2.3	13.9	57.6	20.8	107.1	50.3	10.3	1.8	4.6	15.7	6.1	1.8	188.3	1.29	0.18
	Sample	10	10	10	10	10	10	10	10	10	10	1	1	10	10	10
Granitoid	Minimum	8.6	10.3	10.0	0.7	5.6	7.5	2.7	1.0	3.5	4.0	24.8	1.8	0.6	4.51	0.16
	Maximum	36.7	77.0	67.8	74.1	31.3	50.6	13.8	4.4	6.3	51.0	61.9	9.1	136.6	9.04	0.85
	Mean	22.6	43.2	41.7	22.1	13.8	23.3	7.3	2.6	4.7	11.4	35.8	6.0	91.9	7.32	0.40
	Sample	31	31	31	30	31	31	31	28	20	31	15	15	25	31	31
Endoskarn	Minimum	0.5	2.2	34.5	1.5	14.3	6.7	0.4	1.0	2.6	2.6	12.5	2.9	62.0	0.18	0.00
	Maximum	18.3	105.2	70.7	2.1	359.4	57.2	12.7	14.3	7.9	35.7	20.6	4.0	112.0	1.62	0.06
	Mean	8.6	28.0	56.3	1.8	143.1	32.0	8.1	5.0	4.8	16.5	16.6	3.4	93.2	0.54	0.03
	Sample	6	6	6	4	6	6	6	6	5	6	2	2	6	6	6
Exoskarn	Minimum	0.4	2.1	1.5	2.0	1.9	15.0	0.3	0.8	1.5	12.4	0.8	0.1	12.8	0.1	0.01
	Maximum	114.1	1923.2	148.6	1440.1	289.5	248.5	23.0	15.6	15.7	1098.0	83.6	1.0	169.4	2.2	0.9
	Mean	12.9	177.1	54.4	108.0	38.4	96.0	11.3	5.9	6.9	183.6	42.4	0.6	37.9	0.3	0.2
	Sample	20.0	22.0	22.0	21.0	21.0	22	22	16	17	20	7	3	15	22.0	20.0

Table 2. Continued.

Rock/Alteration		Th	Pb	Zn	Cu	Ni	Co	U	Sn	Mo	As	Nd	Sm	V	Na_2O+K_2O	Rb/Sr
		ppm	ppm	ppm	ppm	ppm	ppm	ppm	ppm	ppm	ppm	ppm	ppm	ppm	ppm	
Ore (Magnetite)	Minimum	0.4	291.0	50.2	45.3	14.7	53.4	0.7	1.0	14.1	2.7	1.0	0.2	21.0	0.06	0.02
	Maximum	4.0	291.0	192.0	45.3	14.7	166.0	8.4	22.2	14.1	33.0	82.3	0.2	21.0	0.16	0.03
	Mean	2.2	291.0	121.1	45.3	14.7	109.7	4.5	11.6	14.1	17.8	41.6	0.2	21.0	0.11	0.03
	Sample	2	1	2	1	1	2	2	2	1	2	2	1	1	2	2

Table 3. Mass balance calculation for major oxides and trace elements.

	SiO_2	TiO_2	Al_2O_3	Fe_2O_3	MnO	MgO	CaO	Na_2O	K_2O	P_2O_5	Ba	Rb	Sr	Y
Granitoid vs endoskarn	6.33	0.10	-1.62	8.64	0.18	9.09	18.15	-2.26	-4.26	-0.01	-911.28	-153.83	232.6	-4.07
Granitoid vs ore	24.80	-0.08	-7.83	1155.57	68.69	29.50	165.35	-1.54	-4.03	0.02	-931.69	-110.38	1738.25	-8.45
Marble vs exoskarn	-0.71	-0.01	-0.02	2.77	-0.19	0.63	-51.45	-0.06	0.02	0.00	-14.94	0.25	-60.11	-11.7
Marble vs ore	-3.43	-0.02	-0.43	28.45	1.56	0.57	-50.84	-0.05	0.01	0.00	-18	0.24	-19.75	-12.15
Mafic-ultramafic vs exoskarn	-9.08	-0.15	-7.00	34.70	0.45	-4.57	19.28	-0.56	-0.31	0.00	-42.38	-6.19	-30.58	-1.65
Mafic-ultramafic vs ore	-32.05	-0.20	-10.51	251.78	15.20	-5.06	24.42	-0.46	-0.44	0.01	-68.25	-6.3	310.53	-5.45
	Nb	Th	Pb	Zn	Cu	Ni	Co	U	Sn	Mo	As	Nd	Sm	V
Granitoid vs endoskarn	0.21	-10.83	-4.99	35.07	-19.69	181.25	20.27	3.73	4.2	1.86	11.14	-13.28	-1.28	35.07
Granitoid vs ore	-3.95	13.86	4742.41	1949.15	722.42	228.14	1780.85	67.25	188.33	227.58	281.78	649.05	-3.49	253.45
Marble vs exoskarn	-2.8	-0.84	-14.33	-4.72	8.03	-52.89	-14.77	-9.11	-0.11	-2.35	29.05	NA	NA	-30.63
Marble vs ore	-3.55	-2.04	82.38	38.73	9.64	-52.92	16.81	-9.03	3.94	2.63	6.14	NA	NA	-27.84
Mafic-ultramafic vs exoskarn	4.48	15.94	236.06	19.16	131.6	-52.93	85.25	5.66	6.56	5.07	243.41	53.77	-0.98	-134.85
Mafic-ultramafic vs ore	-1.84	5.85	1053.56	386.45	145.25	-53.16	352.16	6.35	40.77	47.18	49.7	146.67	-1.25	-111.26

5.2 Comparison of the Kesikköprü granitoid with skarn-related granitoids

The geochemistry of the Kesikköprü granitoid was compared with the global mean, minimum, and maximum values for skarn-related granitoids, as well as with the geochemistry of the Çelebi granitoid [30],[32],[41],[43] (Figure 11).

The SiO_2 contents of the Kesikköprü granitoid range from 58.2 to 69.1% (mean 63.2%) (Table 2). These intervals are broadly consistent with Fe- (47-75.6%), Au- (48.8-68.4%), Cu- (55.7-72.8%), Pb-Zn- (56.7-77%), and W-skarn (53.7-76.4%) granitoids, but are for the most part inconsistent with Mo- (65.3-77.1%) and Sn-skarn (65.3-77.1%) granitoids (Figure 11a).

MgO contents vary between 0.7 and 4.7% (mean 2.2%) (Table 2). These values agree well with Fe- (0.2-7.9%) and Pb-Zn-skarn (0-4.2%) granitoids and are partly consistent with Au- (1.5-5.6%), Cu- (0.5-3.9%), and W-skarn (0-3.6%) granitoids; however, they differ markedly from Mo- (0-2.7%) and Sn-skarn (0-1.1%) granitoids (Figure 11a). On the SiO_2 vs MgO diagram, the Kesikköprü granitoid plots close to the means of Fe-, Au-, and Cu-skarn granitoids and to the Çelebi granitoid (Figure 11a).

K_2O contents range from 1.5 to 5.7% (mean 4.6%), resembling those of Fe- (0.2-5.6%), Cu- (2-5.5%), and Pb-Zn-skarn (1.9-10%) granitoids, and are partly compatible with Au- (0.6-4%), W- (2.5-6.3%), Mo- (2.8-8.5%), and Sn-skarn (2.7-6%) granitoids (Table 2 and Figure 11b). On the SiO_2 vs K_2O diagram, the Kesikköprü granitoid shows values close to the mean values of Cu- and Pb-Zn-skarn granitoids and to the Çelebi granitoid (Figure 11b).

Total alkali of Kesikköprü granitoid (Na_2O+K_2O) ranges from 4.5 to 9% (mean 7.3%) (Table 2). These intervals are comparable to Fe- (0.8-13.1%), Cu- (3.1-10.5%), Pb-Zn- (2-14.7%), W- (4.4-11.8%), Mo- (3-13.4%), and Sn-skarn (3-10.5%) granitoids, and are partly consistent with Au-skarn granitoids (2.8-7.9%) (Figure 11c). On the SiO_2 vs Na_2O+K_2O diagram, the Kesikköprü granitoid yields mean values close to the Fe-, Au-, and Cu-skarn granitoids and to the Çelebi granitoid (Figure 11c).

Zr contents range from 136.3 to 267 ppm (mean 178.1 ppm) (Table 2). These values are similar to those of Cu-skarn granitoids (79-363 ppm) and partly overlap those of Fe- (66-227 ppm), Au- (1-190 ppm), Pb-Zn- (93-188 ppm), W- (42-226 ppm), Mo- (60-186 ppm), and Sn-skarn (27-230 ppm) granitoids (Figure 11d). Rb/Sr ratios vary from 0.16 to 0.85 (mean 0.40) (Table 2). These values are similar to those of Pb-Zn- (0.1-2.3), W- (0.1-26), Mo- (0.1-22.5), and Sn-skarn (0.8-240.2) granitoids, and are partly consistent with Fe- (0-0.45), Au- (0-0.3), and Cu-skarn (0.1-0.5) granitoids (Figure 11d). On the Zr vs Rb/Sr diagram, the Kesikköprü granitoid plots close to the means of Cu- and Pb-Zn-skarn granitoids and to the Çelebi granitoid (Figure 11d).

Ba contents range from 291.8 to 1249 ppm (mean 981 ppm; Table 2). These values are similar in range to W-skarn granitoids (142-2348 ppm) and are partly consistent with Fe- (1-658 ppm), Au- (483-1500 ppm), Cu- (787-2562 ppm), Pb-Zn- (980-1401 ppm), Mo- (376-1449 ppm), and Sn-skarn (14-829 ppm) granitoids (Figure 11e).

On the Zr vs Ba diagram, the Kesikköprü granitoid plots close to the Cu- and Pb-Zn-skarn granitoids and to the Çelebi granitoid (Figure 11e). On the tectonic discrimination diagram [44],[45], the Kesikköprü granitoid plots with granitoids associated with mostly Fe-, Cu-, and Pb-Zn-skarns, consistent with the other diagrams (Figure 11f).

Fe_2O_3 contents range from 1.8 to 6.6% (mean 4.4%) (Table 2). These intervals show strong agreement with Fe- (0.5-6.5%) and Au-skarn (0.6-8.7%) granitoids and with the Çelebi granitoid, and are partly consistent with Cu- (0.8-4.8%), Pb-Zn- (0.3-3.5%), W- (0.2-4.4%), Mo- (0.5-1.9%), and Sn-skarn (0-4.1%) granitoids (Figure 12a).

The Cu contents of the Kesikköprü granitoid range from 0.7 to 74.1 ppm, with a mean of 22.1 ppm (Table 2). These values overlap with the ranges reported for Fe- (0-196 ppm), Cu- (0-1669 ppm), and the Çelebi granitoid, while showing partial consistency with Au- (5-329 ppm), Pb-Zn- (3-420 ppm), W-skarn (5-158 ppm), Mo- (2-9 ppm), and Sn-skarn (3-80 ppm) granitoids (Figure 12b).

Pb contents vary between 10.3 and 77 ppm, averaging 43.2 ppm (Table 2). This range is comparable to Cu- (1-70 ppm) and Pb-Zn-skarn (3-630 ppm) granitoids, while being only partly consistent with Fe- (0-40 ppm), Au- (3-25 ppm), W- (13-270 ppm), Mo- (3-30 ppm), and Sn-skarn (25-3109 ppm) granitoids (Figure 12c).

Zn contents range from 10 to 67.8 ppm, with a mean of 41.7 ppm (Table 2). These values resemble those of W- (10-320 ppm) and Sn-skarn (6-1662 ppm) granitoids, while showing partial overlap with Fe- (25-91 ppm), Au- (29-97 ppm), Cu- (22-98 ppm), Pb-Zn- (45-2080 ppm), and Mo-skarn (4-52 ppm) granitoids (Figure 12d).

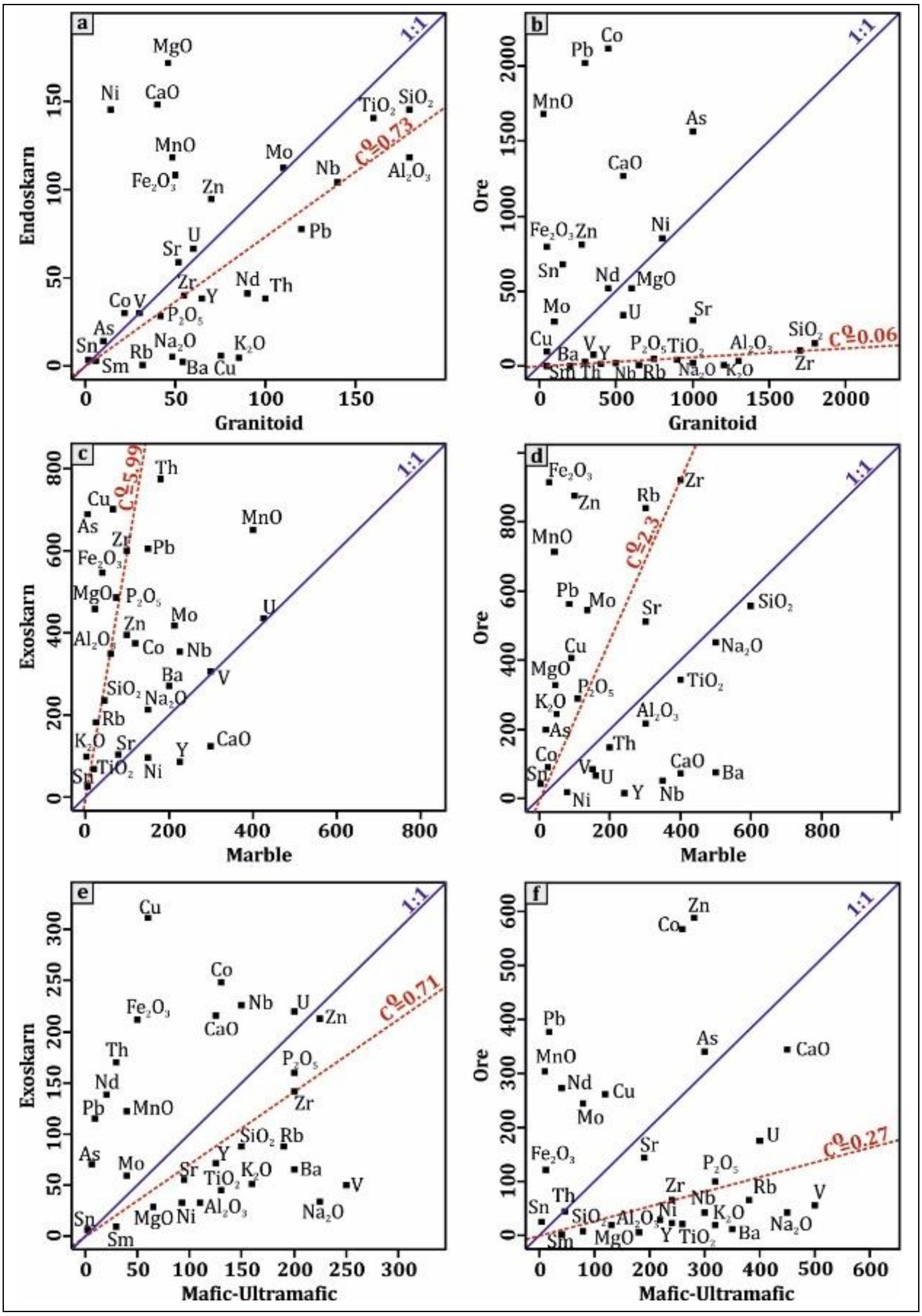

Figure 9. Isocon diagrams. (a): Granitoid vs endoskarn. (b): Granitoid vs ore. (c): Marble vs exoskarn. (d): Marble vs ore. (e): Mafic-ultramafic vs exoskarn. (f): Mafic-ultramafic vs ore.

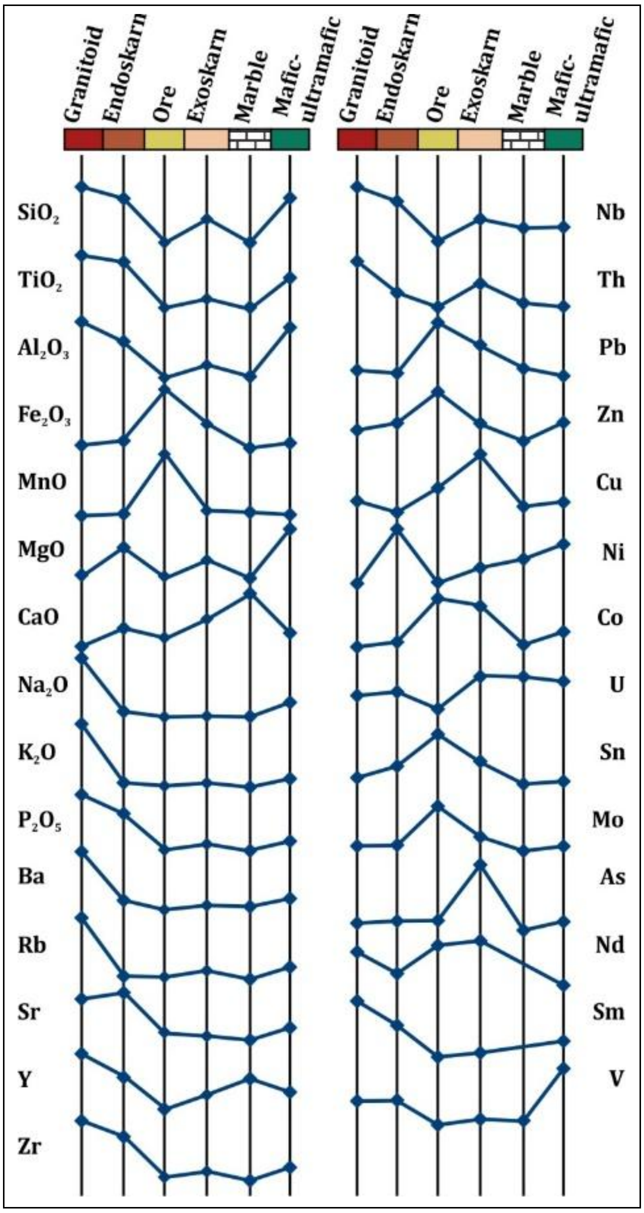

Figure 10. Mean geochemical variations among granitoid, endoskarn, exoskarn, ore zones, and wall rocks.

6 Discussion

6.1 Alteration mineralogy and geochemistry

The Kesikköprü deposit shows a zoned skarn evolution from endoskarn (garnet-pyroxene ± phlogopite ± epidote) to outward–progressing exoskarn subzones (roughly garnet-pyroxene-epidote), with a overprinted by tremolitization chloritization, carbonatization, silicification. Magnetite occurs throughout, but the economic, massive ores are concentrated in the epidote-garnet and epidote exoskarn subzones, where coarse phlogopite is common-consistent with Fe–oxide deposition during the retrograde stage as hydrous fluids overprinted the prograde calc–silicate assemblages. Normally, identification of micas ideally rests on chemical data that demonstrate octahedral Mg dominance (phlogopite) versus Fe^{2+} dominance (annite). In our samples, pervasive alteration, especially chloritization, prevented the acquisition of reliable SEM-EDS analyses, yielding no robust compositions. Comparable difficulties have been reported by Yılmazer & Terzi [3] where extensive alteration hindered geochronology. Despite this limitation, we retain the term phlogopite as an interpretive, context-supported designation for three reasons. (i) Paragenetic context: coarse micas intimately associated with magnetite during the retrograde skarn stage are widely documented as phlogopite in Fe-skarn systems [46]-[50]. (ii) Lithologic and mineralogical context: the occurrence within Mg-rich wall rocks (mafic-ultramafic rocks) and the coexisting magnesian skarn assemblage (forsterite and diopside; [21]) indicate elevated Mg activities in the hydrothermal system, consistent with Mg-dominant mica. (iii) Alteration products: the observed, abundant chloritization and the presence of montmorillonite and vermiculite, confirmed by XRD analyses, are typical of retrograde replacement of Mg-rich biotite in skarns and are consistent with the textural relationships (Figure 4b, e and Figure 5d).

Geochemical assessments of fresh and altered rocks in the Kesikköprü area indicate that skarn samples display variable enrichment-depletion trends relative to the protolith composition of their wall rock lithologies (Figure 9 and Figure 10). A uniform or systematic enrichment-depletion pattern is not consistently observed across all samples. Nonetheless, certain elemental transfers between the wall rock, skarn, and ore zones can be delineated as characteristic features. Endoskarn samples yield clearer geochemical signatures of enrichment-depletion behavior, whereas exoskarn or ore zone samples display distinct patterns of element mobility when compared to the protolith composition.

In the endoskarn zone, bulk mass transfer-driven by Ca-Fe-Mg-Mn-Si addition and coupled Al and alkalis depletion is consistent with feldspar breakdown and the introduction of calc-silicate assemblages (e.g., diopside-hedenbergite, andradite-grossular, amphibole, and epidote) along the intrusive contact (Table 3 and Figure 9a). Strong Rb-Ba and moderate Cu-depletions may reflect LILE removal from feldspars, and biotite breakdown, respectively. One of the important points here is that the V and Ni elements show enrichment in the endoskarn and ore zone samples, which may indicate leaching of these elements from mafic-ultramafic rocks and their addition to the endoskarn zone (Figure 9a, b). In the marble vs exoskarn and ore zone diagrams, the steep isocons and pronounced Ca losses record decarbonation-dominated mass loss (Figure 9c, d). Fe gains reflect the replacement of carbonate by Fe-bearing minerals. With progression into ore, Fe addition intensifies, and the increase in base metals (Zn, Pb, and Co) becomes more evident (Figure 9d). In the mafic-ultramafic-related exoskarn and ore diagrams, the isocons show substantial bulk mass gain. The mass transfer suggests the formation of Fe- and Ca-rich calc-silicates and magnetite through the consumption of silicate phases in the mafic-ultramafic protolith, reflecting extensive replacement by magnetite and calc-silicates. Most trace elements (Pb, Zn, Cu, Co, U, Th, Mo, As, Nd, and Sn) are enriched in the exoskarn and ore zone samples, consistent with introduction and transport by magmatic-hydrothermal (granitic) fluids into reactive mafic-ultramafic rocks (Figure 9e, f). Ni (-52.93 and -53.16) and V (-134,85 and -111.26) show the coherent depletions.

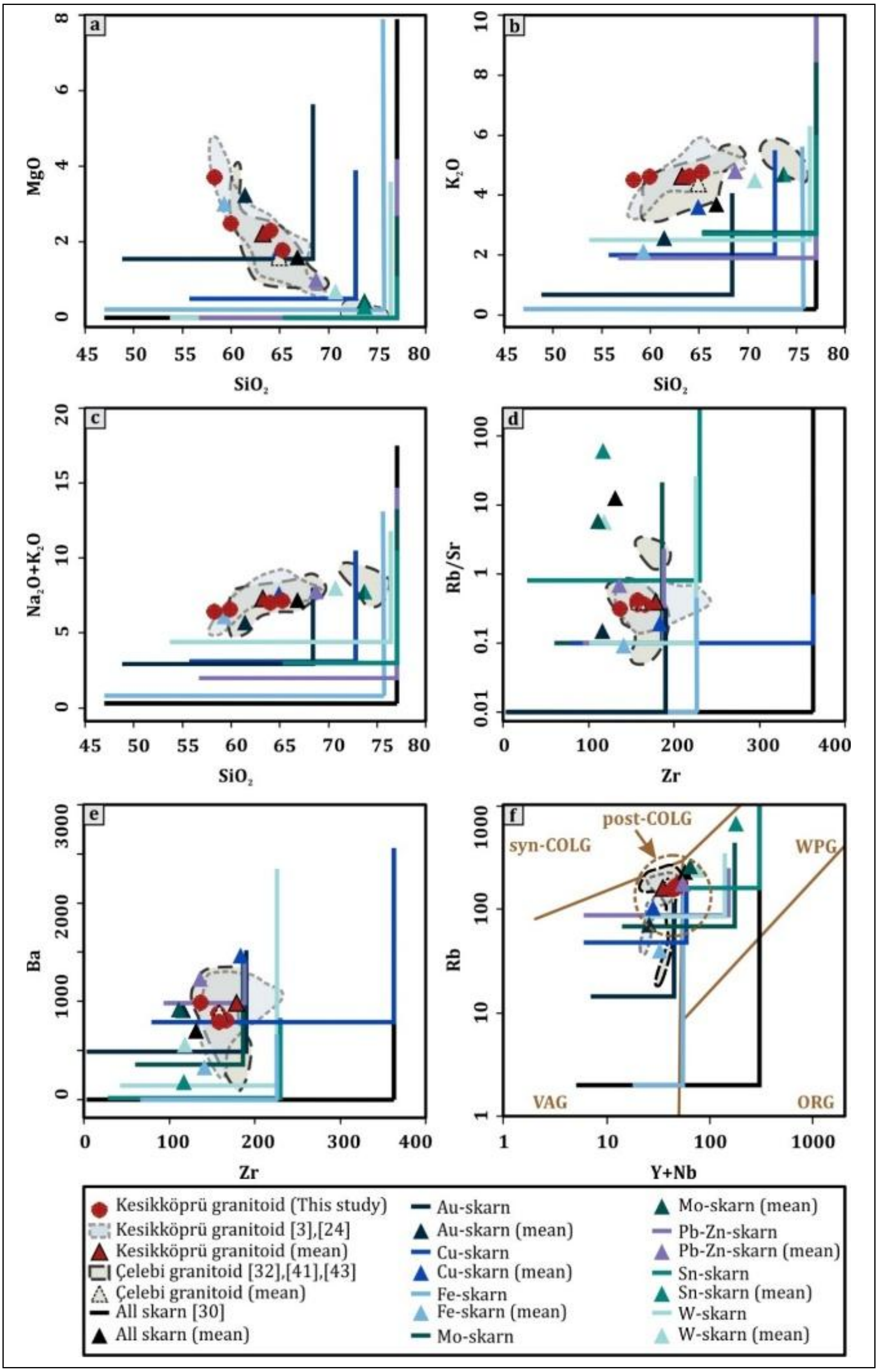

Figure 11. Comparison of Kesikköprü granitoid [3],[24],[This study] with skarn-related granitoids in the world [30] and Çelebi granitoid [32],[41],[43]. (a): SiO_2 vs MgO. (b): SiO_2 vs K_2O. (c): SiO_2 vs Na_2O+K_2O. (d): Zr vs Rb/Sr. (e): Zr vs Ba. (f): Rb vs Y+Nb [44],[45] (ORG: Ocean ridge granite; post-COLG: Post-collision granitoid; Syn-COLG: syn-collision granite; VAG: Volcanic arc granite; WPG: Within-plate granite).

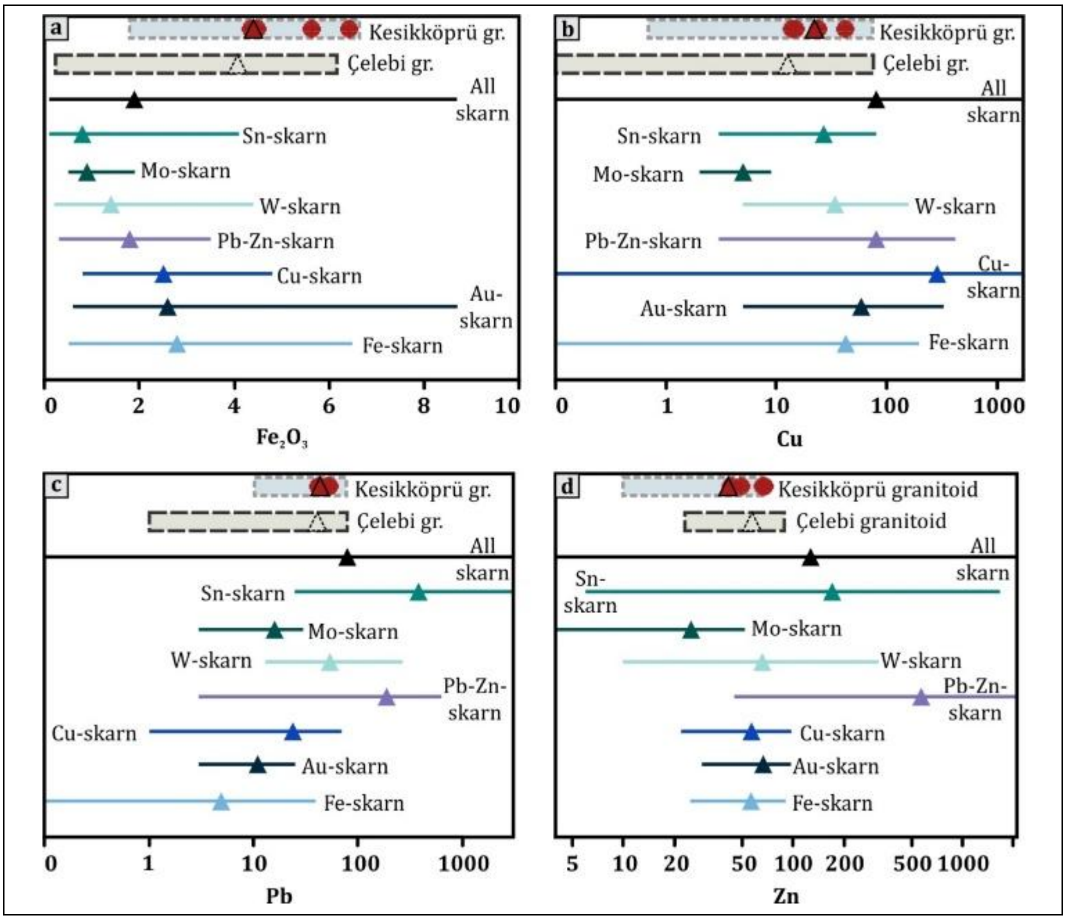

Figure 12. Comparison of the Kesikköprü granitoid [3],[24],[This study] with skarn-related granitoids in the world [30] and the Çelebi granitoid [32],[41],[43]. (a): Fe2O3. (b): Cu. (c): Pb. (d): Zn (See Figure 11 for legend explanation).

This is consistent with mafic-ultramafic mineral breakdown and redistribution into the endoskarn zone, where Ni and V can be mobilized or partitioned into phases not stabilized in the exoskarn zone (Table 3).

Collectively, the isocon slopes and mass balance calculations define a mass transfer regime: (i) granitoids undergo Al and alkali leaching concurrent with Ca-Fe-Mg-Mn-Si addition to produce endoskarn; (ii) marbles experience decarbonation-driven mass loss during exoskarn and ore development, with incremental Fe addition toward ore; and (iii) mafic-ultramafic rocks are highly receptive to Fe, Ca, and base metal input in both the exoskarn and ore zones, yielding exceptionally elevated metal budgets in the ore zone. Additionally, LILE depletion (Rb, Ba) in the endoskarn and exoskarn zones reflects feldspar and/or carbonate breakdown, whereas chalcophile and transition metal enrichments (Zn, Cu, Co, Pb, and partly V) may indicate the input of ore fluids and the newly formed skarn and magnetite.

Mineral-chemistry analyses of garnet indicate decreasing grossular and increasing andradite from crystal cores toward rims [21]. This trend suggests a progressive decrease in Al and an increase in Fe in hydrothermal fluids from the endoskarn to the exoskarn zone (Figure 10). The gradual decrease of Al_2O_3 toward the ore and exoskarn zones is, in turn, directly related to drop in grossular-rich garnets and/or the corresponding increase in andraditic garnets [51] as the SEM–EDS results of garnets imply the decrease in Al contents (from 1.62-2.94% to 0.30-2.78%) and increase in Fe content (from 18.15-20.30% to 18.64-23.07%) from the garnet (±pyroxene±phlogopite) to the epidote-garnet exoskarn subzone (Figure 5c and Figure 7c).

From granitoid toward endoskarn, ore, and exoskarn zones, SiO_2 contents decrease in parallel with Al_2O_3 (Figure 10). This depletion is consistent with the incorporation of Si into diopsidic pyroxene and with the use of Si and Al in the formation of grossular-rich garnet, epidote, and phlogopite. The Mg required for the formation of diopsidic pyroxene and phlogopite could have been possibly derived from mafic-ultramafic rocks (up to 18.1% MgO) (Table 2). The Ca required for pyroxene, garnet, and epidote formation was likely supplied by marbles, which contain 55.3% CaO, consistent with the increase in CaO from granitoid toward the endoskarn and exoskarn zones (Table 2, Figure 9 and Figure 10). The low Fe and Mn but high Mg contents of pyroxenes suggest that Mg was present in the early hydrothermal fluids and that high Mg activity prevailed during the early stages of skarn formation [21],[52]. This may indicate that Mg was supplied directly from granitoid (up to 4.7% MgO) and/or leached from the mafic-ultramafic rocks through fluid-rock interaction. Bayhan [21] also reported the presence of forsterite in alteration assemblages at Kesikköprü and noted that its formation required the remobilization of Mg and Si from the wall rocks.

Given that the iron enrichment is especially concentrated in the epidote-garnet and epidote exoskarn subzones, suggests the increased Fe input during the later stages of skarn evolution [3],[21]. The occurrence of early-stage pyroxenes with diopside, salite, and fassaite compositions, the progressive increase in andradite contents from garnet cores to rims, and the formation of pistacite-rich epidotes in the epidote-garnet and epidote exoskarn subzones collectively indicate that Fe content was relatively low during the early stages of skarn formation but increased toward later stages and into the wall rocks [21]. This also suggests that Fe may initially have been leached from granitoid and/or mafic-ultramafic rocks during early skarn formation. In particular, the breakdown of ferromagnesian minerals such as olivine and pyroxene in the mafic-ultramafic lithologies may be an important source of Fe [25],[26],[53]. The enrichment of Fe in the endoskarn, ore, and exoskarn zones relative to their protoliths, however, might suggest that multiple sources contributed to the deposit's Fe budget (Figure 9 and Figure 10). To refine source contributions and fluid evolution, advanced mineral chemistry (e.g., EMPA) and isotope analyses are warranted. In situ trace-element and isotope studies of magnetite and garnet, in particular, can illuminate fluid-rock interactions and temporal changes in fluid composition during progressive skarn formation.

6.2 Evaluation of the potential of the Kesikköprü granitoid to produce skarn with different metal endowments

Numerous studies have examined the genetic link between the major oxide and trace element geochemistry of skarn-forming granitoids and the metal endowment of the skarns they produce [30]-[33], [54]-[58]. In this context, the major oxide and trace element compositions of the Kesikköprü granitoid were compared with Meinert [30]'s dataset associated with Au-, Cu-, Fe-, Mo-, Pb-Zn-, Sn-, and W-skarns, as well as with the geochemistry of the Fe- and Fe-W skarn related Çelebi granitoid [32],[41],[43] (Figure 11 and Figure 12). Geochemically, when evaluated against skarn-related granitoids worldwide, the Kesikköprü granitoid falls within the range typical of Fe-skarn granitoids and shows particularly close affinities to Cu-skarn granitoids, with partial overlap with those linked to Au and Pb-Zn skarns (Figure 11 and Figure 12). Although copper and gold mineralization have not yet been documented at the Kesikköprü Fe-skarn deposit, late-stage phases (calcite-, quartz-, and sulfide-bearing veins) related to the Kesikköprü and Çelebi granitoids contain concentrations that may be considered anomalous [55],[59], with 1-2% Cu, 1,500 ppb Au, and up to 2,777 ppm As [3],[15],[20],[29],[32]. Moreover, in light of the geochemical characteristics, tectonic setting, and age relations [3],[32],[41],[43], together with the occurrence of Pb-Zn veins within the Kesikköprü granitoid and the presence of Pb-Zn skarn (Keskin) and porphyry Cu-Mo (Karacaali, Balışeyh) systems in the region [22],[27],[60],[61], the Kesikköprü granitoid may have the potential to generate skarns with different metal endowments. Therefore, despite the current lack of direct evidence, this region should not be overlooked, particularly with respect to possible Cu, Au, and Pb-Zn enrichment.

7 Conclusions

The Kesikköprü Fe-skarn deposit consists of an endoskarn represented by a garnet-pyroxene (±phlogopite±epidote) assemblage and four exoskarn subzones-garnet (±pyroxene ±phlogopite), pyroxene (±garnet±phlogopite±epidote), epidote-garnet, and epidote. Exoskarns cover a larger area than the endoskarn zone, with economic iron mineralization concentrated in the epidote-garnet and epidote exoskarn subzones. Alteration mineralogy and geochemical patterns demonstrate that protolith composition strongly controls skarn mineralogy, elemental redistribution, and ore localization.

Mass-balance and transect data indicate that i) granitoids gain Ca-Fe-Mg-Mn-Si with Al and alkali loss to form calc-silicate minerals in the endoskarn zone; ii) marbles undergo decarbonation with Fe input and later Fe enrichment in the ore zone; and iii) mafic-ultramafic rocks are highly receptive to Fe and Ca input, developing metal-rich signatures with Pb-Zn-Cu-Co enrichment and Ni-V depletion. Depletion of LILEs (Rb, Ba) reflects the breakdown of feldspar and carbonate. Garnet zoning from grossular to andradite and Fe-rich epidote compositions support increased magnetite mineralization in epidote-garnet and epidote subzones. MgO enrichments point to the formation of diopsidic pyroxene, phlogopite, and tremolite, consistent with the mafic-ultramafic protolith.

Geochemically, the Kesikköprü granitoid resembles granitoids associated with Fe- and Cu-skarns, and to a lesser extent those linked to Au- and Pb-Zn-skarns. This suggests a magmatic source capable of generating skarns with diverse metal contents. Although there is no direct evidence of Cu, Au, Pb, and Zn mineralization at Kesikköprü, the presence of Cu, Au, and As anomalies in late-stage veins and nearby Pb-Zn veins, Pb-Zn skarns, and porphyry Cu-Mo systems reported in the literature highlights the broader metallogenic potential of the Kesikköprü region.

8 Acknowledgement

This manuscript is derived from the MSc thesis of the first author, conducted under the supervision of the second author, and was financially supported by the Research Fund of Aksaray University (Project numbers: 2013-079, 2015-028, and 2018-009). The authors express their sincere gratitude to Özce and Güncem Mining Companies for providing logistical assistance during the fieldwork. The authors also gratefully acknowledge the three anonymous reviewers for their insightful and constructive comments, which helped improve the quality and clarity of the manuscript.

9 Author contribution statements

Conceptualization, methodology, investigation, writing-original draft, writing-review and editing, visualization (Mustafa Haydar Terzi and Erkan Yılmazer), and supervision (Erkan Yılmazer).

10 Ethics committee approval and conflict of interest statement

"Ethics committee approval was not required for the preparation of this article". "The authors declare no conflict of interest with any individual or institution in relation to the preparation of this article."

11 References

[1] Göncüoğlu MC, Toprak V, Kuşcu İ, Erler A, Olgun E. "Orta Anadolu Masifinin Batı Bölümünün Jeolojisi, Bölüm 1-Güney Kesim". Türkiye Petrolleri Anonim Ortaklığı, Ankara, Türkiye, 2909, 1991.

[2] Kuşcu İ, Erler A. "Mineralization events in a collision related setting: The Central Anatolian Crystalline Complex". *International Geology Review*, 40(6), 552-565, 1998.

[3] Yılmazer E, Terzi MH. "Geochemistry, isotope characteristics, and evolution of the Kesikköprü iron deposit (Türkiye)". *Minerals*, 15(5), 528, 2025.

[4] Maden Tetkik ve Arama Genel Müdürlüğü, *Türkiye Yer Altı Kaynakları (İllere göre)*. MTA Yer Bilimleri ve Kültür Serisi-5, Ankara, Türkiye, 2009.

[5] Brennich G. "Çelebi-Kesikköprü-Hirfanlı Bölgesinde Manyetit Zuhurları Hakkında Rapor". Maden Tetkik ve Arama Genel Müdürlüğü, Ankara, Türkiye, 2755, 1960.

[6] Kraeff A. "Kesikköprü Konsesyonu". Maden Tetkik ve Arama Genel Müdürlüğü, Ankara, Türkiye, 3349, 1962.

[7] Boroviczeny F. "200/240 No.lu Ruhsat Sahasının Kesikköprü Yakınındaki Demir Yatağı Hakkındaki Rapor". Maden Tetkik ve Arama Genel Müdürlüğü, Ankara, Türkiye, 3481, 1964.

[8] Boroviczeny F. "200/212 Nolu Ruhsat Sahasında Yapılan Jeolojik Etüdler Hakkında Sunulan Rapor". Maden Tetkik ve Arama Genel Müdürlüğü, Ankara, Türkiye, 3570, 1964.

[9] Boroviczeny F. "Kesikköprü Yakınındaki 200/240 No.lu Ruhsat Sahasında Yapılan Jeolojik Etüdler Hakkında Rapor". Maden Tetkik ve Arama Genel Müdürlüğü, Ankara, Türkiye, 3591, 1964.

[10] Boroviczeny F. "200/248 Nolu Ruhsat Sahasında Yapılan Jeolojik Etüdler Hakkında Sunulan Rapor". Maden Tetkik ve Arama Genel Müdürlüğü, Ankara, Türkiye, 3584, 1964.

[11] Yaz N, Sözen A. "Kesikköprü Madencilik Ltd. Şirketi Kesikköprü Demir Ruhsat Sahaları Hakkında Rapor". Maden Tetkik ve Arama Genel Müdürlüğü, Ankara, Türkiye, 3810, 1965.

[12] Yaz N, Sözen A. "Kesikköprü-Çelebi-Hirfanlı Bölgesinin Manyetit+Hematit Zuhurları Hakkında Rapor". Maden Tetkik ve Arama Genel Müdürlüğü, Ankara, Türkiye, 4440, 1967.

[13] Sözen A. "Kesikköprü Madentepe Manyetit Zuhur Hakkında Rapor". Maden Tetkik ve Arama Genel Müdürlüğü, Ankara, Türkiye, 4212, 1970.

[14] Sungurlu B. "Kesikköprü-Çelebi-Hirfanlı Bölgesinin Manyetit Zuhurları Hakkında (Yaz ve Sözen) İsimli Rapordan Kesikköprü Ltd. Şirketine ait Ar: 200/248 Ruhsat No'lu Demir Sahası İçin Derlenen Rapordur". Maden Tetkik ve Arama Genel Müdürlüğü, Ankara, Türkiye, 4231, 1970.

[15] Öztürk M. "Ankara-Keskin-Çelebi; Kırşehir-Kaman; Nevşehir-Hacıbektaş Yörelerindeki Demir Zuhurlarının Jeoloji Raporu". Maden Tetkik ve Arama Genel Müdürlüğü, Ankara, Türkiye, 7158, 1981.

[16] Öztürk K, Kurt M, Öztürk M, Sarı İ. "Ankara-Bala-Kesikköprü, Madentepe, Büyükocak, Çataldere, Camiisagir Demir Yatakları Jeoloji ve Rezerv Raporu". Maden Tetkik ve Arama Genel Müdürlüğü, Ankara, Türkiye, 7355, 1983.

[17] Öztürk K, Öztürk M. "Ankara-Bala-Yukarıtepeköy-Kartalkaya Demir Cevherleşmesi Jeoloji Etüd ve Arama Raporu". Maden Tetkik ve Arama Genel Müdürlüğü, Ankara, Türkiye, 7357, 1983.

[18] Bilgin ZR, Akarsu B, Erbaş A, Elibol E, Yaşar T, Esentürk K, Güner E, Kara H. "Kırıkkale-Kesikköprü-Çiçekdağı Alanının Jeolojisi". M.T.A Derleme Rapor No: Maden Tetkik ve Arama Genel Müdürlüğü, Ankara, Türkiye, 7876, 1986.

[19] Demiröz T, Ceylan Ü, Okşaş M. "Kesikköprü-Bala-Ankara Madentepe Büyükocak Boyalı İn Demir Yatakları Fizibilite Etüdü". Maden Tetkik ve Arama Genel Müdürlüğü, Ankara, Türkiye, 8286, 1986.

[20] İşbaşarır O, Arda N, Tosun S. "Kesikköprü (Bala-Ankara) Demir Yatağı Maden Geçidi, Suluocak ve Boyalı İn Ocağı Detay Jeoloji ve Jeofizik Raporu". Maden Tetkik ve Arama Genel Müdürlüğü, Ankara, Türkiye, 10649, 2004.

[21] Bayhan H. "Kesikköprü skarn kuşağının (Bala-Ankara) mineralojisi ve petrojenezi". *Hacettepe Üniversitesi Yerbilimleri*, 11, 45-57, 1984.

[22] Bayhan H. "Kesikköprü (Bala-Ankara) yöresindeki Fe, Pb-Zn ve florit cevherleşmelerinin mineralojisi". *Cumhuriyet Üniversitesi Mühendislik Fakültesi Dergisi*, Seri A-Yerbilimleri, 6-7(1-2), 25-33, 1990.

[23] Wondenmagegnahu TW. Mineralogy, Chemistry and Physical Properties of the Magnetite Ore Deposits Around Kesikköprü Village and the Surrounding Areas. MSc Thesis, Middle East Technical University, Ankara, Türkiye, 1990.

[24] Terzi MH. Kesikköprü (Bala-Ankara) Demir-Oksit Cevherleşmelerinin Mineralojisi, Petrografisi ve Jeokimyası. Yüksek Lisans Tezi, Aksaray Üniversitesi, Aksaray, Türkiye, 2014.

[25] Doğan B. Kesikköprü Demir Yatağının (Bala-Ankara) Maden Jeolojisinin İncelenmesi. Yüksek Lisans Tezi, Ankara Üniversitesi, Ankara, Türkiye, 1996.

[26] Doğan B, Ünlü T, Sayılı S. "Kesikköprü (Bala-Ankara) demir yatağının kökenine bir yaklaşım". *Bulletin of the Mineral Research and Exploration*, 120, 1-33, 1998.

[27] Kuşcu İ, Tosdal RM, Gençalioğlu-Kuşcu G. "Episodic porphyry Cu (-Mo-Au) formation and associated magmatic evolution in Turkish Tethyan collage". *Ore Geology Reviews*, 107, 119-154, 2019.

[28] Orhan A, Deniz K. "Kaman Fe-skarn yatağı ile ilişkili Çelebi Plütonu'nun jeokimyası, mineral kimyası ve kristallenme koşulları (Kırşehir, Orta Anadolu)". *Uluslararası Katılımlı 73. Türkiye Jeoloji Kurultayı*, Ankara, Türkiye, 24-28 Mayıs 2021.

[29] Orhan A. "Mineralogy, fluid inclusions and carbon isotopes of the Kaman iron deposits, Central Anatolia, Turkey: Implication for ore genesis and hydrothermal evolution". *Ore Geology Reviews*, 127, 103808, 2020.

[30] Meinert LD. Compositional Variation of Igneous Rocks Associated with Skarn Deposits-Chemical Evidence for a Genetic Connection Between Petrogenesis and Mineralization. Editor: Thompson JFH. Magmas, Fluids, and Ore Deposits, Mineralogical Association of Canada Short Course Series, 23, 401-418, Victoria, British Columbia, Canada, Mineral Deposit Research Unit Press, 1995.

[31] Kuşcu İ, Gençalioğlu-Kuşcu G, Erler A. "Geochemical signatures of granitoids associated with skarns in central Anatolia". *International Geology Review*, 43(8), 722-735, 2001.

[32] Kuşcu İ, Gençalioğlu-Kuşcu G, Meinert LD, Floyd PA. "Tectonic setting and petrogenesis of the Çelebi granitoid, (Kırıkkale-Turkey) and comparison with world skarn granitoids". *Journal of Geochemical Exploration*, 76(3), 175-194, 2002.

[33] Kuşcu İ, Gençalioğlu-Kuşcu G, Sarac C, Meinert LD. "An approach to geochemical characterization of productive versus barren granitoids in terms of iron in Central Turkey". *Journal of Asian Earth Sciences*, 24(3), 311-325, 2004.

[34] Seymen İ. "Kaman (Kırşehir) dolayında Kırşehir masifinin stratigrafisi ve metamorfizması". *Türkiye Jeoloji Kurumu Bülteni*, 24, 7-14, 1981.

[35] Göncüoğlu MC, Toprak V, Kuşcu İ, Erler A, Olgun E, Rojay B. "Orta Anadolu Masifinin Batı Bölümünün Jeolojisi, Bölüm 2: Orta Kesim". Türkiye Petrolleri Anonim Ortaklığı, Ankara, Türkiye, 3155, 1992.

[36] Göncüoğlu MC, Erler A, Toprak V, Olgun E, Yalınız K, Kuşcu İ, Köksal S, Dirik K. "Orta Anadolu Masifi'nin Orta Bölümü'nün Jeolojisi, Bölüm 3. Orta Kızılırmak Tersiyer Baseni'nin Jeolojik Evrimi". Türkiye Petrolleri Anonim Ortaklığı, Ankara, Türkiye, 3313, 1993.

[37] Akıman O, Erler A, Göncüoğlu MC, Güleç N, Geven A, Türeli TK, Kadıoğlu YK. "Geochemical characteristics of granitoids along the western margin of the Central Anatolian crystalline complex and their tectonic implications". *Geological Journal*, 28(3-4), 371-382, 1993.

[38] Erler A, Bayhan H. "Orta Anadolu granitoyidlerinin genel değerlendirilmesi ve sorunları". *Yerbilimleri*, 17, 49-67, 1995.

[39] Işık F, Baş H, Koçak K. "Gabroyik kayaçların petrografik ve jeokimyasal karakteristikleri: Orta Anadolu Masifi, Yeşilhisar-Kayseri (Türkiye)". *Pamukkale Üniversitesi Mühendislik Bilimleri Dergisi*, 8(2), 227-238, 2002.

[40] Bailey EB, Mc Callien WJ. "Ankara melanjı ve Anadolu şariyajı". *Bulletin of the Mineral Research and Exploration*, 40, 17-21, 1950.

[41] Bayhan H. "İç Anadolu granitoyid kuşağındaki Çelebi sokulumunun jeokimyası ve kökensel yorumu". *Jeoloji Mühendisliği*, 29, 27-36, 1986.

[42] Grant JA. "The isocon diagram-a simple solution to Gresens equation for metasomatic alteration". *Economic Geology*, 81, 1976-1982, 1986.

[43] İlbeyli N, Pearce JA, Thirwall MF, Mitchell JG. "Petrogenesis of collision-related plutonics in central Anatolia, Turkey". *Lithos*, 72(3-4), 163-182, 2004.

[44] Pearce JA, Harris NBW, Tindle AG. "Trace-element discrimation diagrams for the tectonic interpretation of granitic rocks". *Journal of Petrology*, 25, 956-983, 1984.

[45] Pearce JA. "Sources and settings of granitic rocks". *Episodes*, 19, 120-125, 1996.

[46] Li W, Xie G, Mao J, Zhu Q, Zheng J. "Mineralogy, fluid inclusion, and stable isotope studies of the Chengchao deposit, Hubei province, eastern China: Implications for the formation of high-grade Fe skarn deposits". *Economic Geology*, 114(2), 325-352, 2019.

[47] Qu H, Friehauf K, Santosh M, Pei R, Li D, Liu J, Zhou S, Wang H. "Middle–Late Triassic magmatism in the Hutouya Fe–Cu–Pb–Zn deposit, East Kunlun Orogenic Belt, NW China: Implications for geodynamic setting and polymetallic mineralization". *Ore Geology Reviews*, 113, 103088, 2019.

[48] Ghinet CS, Marincea S. "Phlogopite in magnesian skarns from seven occurrences in the Banatitic Magmatic and Metallogenetic Belt, Romania". *Goldschmidt Conference*, *Virtual,* 4-9 July 2021.

[49] Kaya M, Kumral M, Yalçın C, Abdelnasser A. "Genesis and evolution of the Yolindi Cu-Fe skarn deposit in the Biga Peninsula (NW Turkey): insights from genetic relationships with calc-alkaline magmatic activity". *Minerals*, 13(10), 1304, 2023.

[50] Feng Q, Gao M, Fu C, Li S, Li Y, Gao J, Ma M, Wang Z, Zhu Y, Wu B, Duan Z, Dang Z. "Phlogopite $^{40}Ar/^{39}Ar$ geochronology for guodian skarn fe deposit in qihe–yucheng district, luxi block, north china craton: a link between craton destruction and Fe mineralization". *Minerals*, 14(7), 690, 2024.

[51] Kuşcu İ. "Geochemistry and mineralogy of the skarns in the Çelebi district, Kırıkkale, Turkey". *Turkish Journal of Earth Sciences*, 10(3), 121-132, 2001.

[52] Yao Y, Chen J, Lu J, Wang R, Zhang R. "Geology and genesis of the Hehuaping magnesian skarn-type cassiterite-sulfide deposit, Hunan Province, Southern China". *Ore Geology Reviews*, 58, 163-184, 2014.

[53] Ünlü T, Dumanlılar Ö, Tosun L, Akıska S, Tiringa D. *Turkish Iron Deposits*. Editors: Pirajno F, Ünlü T, Dönmez C, Şahin MB. Mineral Resources of Turkey, Modern Approaches in Solid Earth Sciences, 16, 225-260, Cham, Switzerland, Springer, 2019.

[54] Einaudi MT, Meinert LD, Newbery RJ. "Skarn deposits". *Economic Geology*, 75th Anniversary Volume, 317-391, 1981.

[55] Meinert, LD, Dipple GM, Nicolescu S. "World skarn deposits". *Economic Geology*, 100th Anniversary Volume, 299-336, 2005.

[56] Demirela G. Orta Anadolu Bölgesinde Demir (Fe) ve Kurşun-Çinko Üreten Skarn Granitoyidlerinin Jeokimyasal Karakterizasyonu ve Farkları. Yüksek Lisans Tezi, Niğde Üniversitesi, Niğde, Türkiye, 2003.

[57] Demirela G, Kuşçu İ, Yılmazer E, Saraç C. "Orta Anadolu bölgesinde yer alan Fe-skarn granitoyidlerinin temel jeokimyasal özellikleri". *Türkiye Demir Yatakları Jeolojisi Madenciliği ve Mevcut Sorunları Sempozyumu*, İstanbul, Türkiye, 23-25 Haziran 2005.

[58] Yücel-Öztürk Y, Helvacı C, Satir M. "Genetic relations between skarn mineralization and petrogenesis of the Evciler Granitoid, Kazdağ, Çanakkale, Turkey and comparison with world skarn granitoids". *Turkish Journal of Earth Sciences*, 14(3), 255-280, 2005.

[59] Meinert LD, Brooks JW, Myers GL. *Whole Rock Geochemistry and Contrast Among Skarn Types*. Editors: Buffa RH, Coyner AR. Geology and Ore Deposits of the Great Basin: Reno, Nevada, Geological Society of Nevada, Fieldtrip Guidebook Compendium, 1, 72-80, 1991.

[60] Delibaş O. Kırıkkale-Yozgat Yöresi Demir, Bakır-Molibden ve Kurşun Cevherleşmelerinin Oluşumunda Magma Karışım Süreçlerinin Rolü. Doktora Tezi, Hacettepe Üniversitesi, Ankara, Türkiye, 2009.

[61] Delibaş O, Genc Y. "Re-Os molybdenite ages of granitoid-hosted Mo-Cu occurrences from central Anatolia (Turkey)". *Ore Geology Reviews*, 44, 39-48, 2012.